Chapter 7

Silver-Antimony-Telluride: From First-Principles Calculations to Thermoelectric Applications

Yaron Amouyal

Additional information is available at the end of the chapter

http://dx.doi.org/10.5772/66086

Abstract

Silver-antimony-telluride ($AgSbTe_2$) based compounds have emerged as a promising class of materials for thermoelectric (TE) power generation at the mid-temperature range. This Chapter demonstrates utilization of first-principles calculations for predicting TE properties of $AgSbTe_2$-based compounds and experimental validations. Predictive calculations of the effects of La-doping on vibrational and electronic properties of $AgSbTe_2$ compounds are performed applying the density functional theory (DFT), and temperature-dependent TE transport coefficients are evaluated applying the Boltzmann transport theory (BTE). Experimentally, model ternary ($AgSbTe_2$) and quaternary (3 at. % La-$AgSbTe_2$) compounds were synthesized, for which TE transport coefficients were measured, indicating that thermal conductivity decreases due to La-alloying. The latter also reduces electrical conductivity and increases Seebeck coefficients. All trends correspond with those predicted from first-principles. Thermal stability issues are essential for TE device operation at service conditions, e.g. changes of matrix composition and second-phase precipitation, and are also addressed in this study on both computational and experimental aspects. It is shown that La-alloying affects TE figure-of-merit positively, e.g., improving from 0.35 up to 0.50 at 260 °C. We highlight the universal aspects of this approach that can be applied for other TE compounds. This enables us screening their performance prior to synthesis in laboratory.

Keywords: silver-antimony-telluride, first-principles calculations, thermoelectric transport properties, Boltzmann transport theory, lattice dynamics, thermal stability

1. Introduction

It is of utmost technological importance to develop predictive tools that will provide us with information about design of materials' functional properties. In this context, density functional theory (DFT) first-principle calculations offer us such possibilities [1–4], allowing us

calculation of structural, interfacial, vibrational, and electronic properties. Knowledge of these properties and how they depend on temperature and material's composition are essential to assess total thermoelectric (TE) performance of thermoelectric device. Among recently investigated TE materials, silver-antimony-telluride ($AgSbTe_2$)-based alloys have emerged as a promising class of materials for TE power generation in low- to mid-temperature range. These compounds are derivatives of lead-antimony-silver-telluride (LAST)-based alloys of $AgPb_mSbTe_{2+m}$ form [5–9], which exhibit large TE figure-of-merit *ZT* values ranging from 1.3 to 1.7 [5, 10, 11], which are associated with the intrinsically good TE properties of $AgSbTe_2$-phase.

$AgSbTe_2$-based alloys serve not only for TE power conversion or cooling, but also for non-volatile electronic memory, being classified as phase change materials, as demonstrated in thorough investigation by Wuttig and coworkers [12–15]. They have attracted scientific interest owing to their special nature of interatomic bonding and vibrational properties [16–18]. On TE aspect, their superior performance is associated mainly to glass-like, intrinsically low values of lattice thermal conductivities, as low as 0.6 $W\ m^{-1}\ K^{-1}$ [19]. This anomaly is associated either to strong anharmonicity of interatomic forces [20, 21] or to relatively large variance of interatomic forces prevailing between Ag^+ and Sb^{3+} cations, encouraging phonon scattering [22]. Additionally, resonant bonding yields high level of structural instability, that is accompanied, for instance, by spontaneous phase decomposition [23, 24]. This, intriguingly, what makes $AgSbTe_2$-based alloys good materials for both TE and phase change applications. Owing to these peculiarities, these alloys have recently been investigated extensively, either experimentally [19, 25–30] or computationally [18, 22, 31–33].

Despite of relatively high *ZT* values of $AgSbTe_2$ phase, it is still challenging to increase them to the range of 2–3. Reaching at this limit will enable us employing this material for energy conversion at power levels >500 W [34]. Reduction in lattice thermal conductivity is a conventional way to enhance TE performance and is achieved by either doping with solute elements [35] or formation of second phases to stimulate phonon scattering [36–38]. These lattice defects affect, of course, electronic properties, mainly electrical conductivity and Seebeck coefficient. Attempts to improve TE properties of $AgSbTe_2$-based alloys by doping with different elements [19, 25, 39–47], as well as, by formation of second phase precipitates [46, 48–51], proved to be successful, as reported in the exhaustive studies of Zhang et al., Du et al., and Mohanraman et al. Alloying with second phase forming elements raises imperative question about material's thermal stability, when employed in TE generators under service conditions, with engineering implications [51–53].

Among efforts to improve TE properties of $AgSbTe_2$-based alloys, Min et al. reported on improvement of electron transport properties due to La-doping [27]. Positive effects on PbTe compound due to La-doping were recorded, as well [54, 55]. In their recent study, Min et al. introduce a complete analysis of TE properties of $AgSbTe_2$ doped with La of different concentrations [56].

Notwithstanding the aforementioned successful experimental and computational attempts, a set of experimental routines, that is initiated and directed by predictions from first principles for complete TE performance or any other computational procedure, is missing.

A significant step in this direction is introduced by our previous investigations of $AgSbTe_2$-based phase, involving both computational and experimental aspects [57, 58]. Vibrational properties of both $AgSbTe_2$-based and La-doped-$AgSbTe_2$ alloys, including frequency-dependent vibrational density of states functions (v-DOS), temperature-dependent heat capacity, sound velocities, and Debye temperatures were evaluated employing lattice dynamics first-principles calculations. It was reported that La-doping reduces average sound velocity and varies v-DOS of $AgSbTe_2$-based phase [57, 58]. Quantitatively, lattice thermal conductivity of $La_{0.125}Ag_{0.875}SbTe_2$ alloy was calculated to be lower by ca. 14%, than that of $AgSbTe_2$-based phase at 300 K [58]. Experimental validations of these effects of La-alloying on reducing lattice thermal conductivity were made, as well [58].

This chapter introduces a refined approach of evaluating temperature-dependent lattice thermal conductivity from data obtained *ab-initio*, as well as, calculations of electronic transport coefficients. Most importantly, this chapter presents experimental validations for the entire dataset obtained from first-principles, including thermal and electrical measurements.

2. Chapter outline

This chapter consists primarily of original computational and experimental data along with data, that were reported by us earlier [57, 58], and is aimed at drawing a complete picture depicting the role of lanthanum-alloying in silver-antimony-telluride-based alloys on a broad TE view. Herein, we demonstrate how alloying of $AgSbTe_2$ (P4/mmm) alloy with lanthanum solute atoms brings about significant reduction in thermal conductivity with positive effects on TE power factor, as well; thus, achieving improved ZT values. This is achieved by DFT calculations of structural, interfacial, vibrational, and electronic properties performed for La-free and La-doped alloys, followed by experimental validation implemented by thermal and electronic transport measurements.

Computational procedures are divided into the following steps:

1. Total energy calculations for different polymorphs of $AgSbTe_2$ phase are implemented to evaluate their Helmholtz free energies, indicating which one is the most stable around and above room temperature.
2. Vibrational calculations are performed for both La-free and La-doped lattices, including phonon dispersion and density of states, average sound velocity, and Debye temperature. These values enable us evaluating temperature-dependent lattice thermal conductivity values.
3. Electronic calculations of band structures of both La-free and La-doped lattices are performed, and the resulting transport coefficients are derived applying Boltzmann transport theory.
4. To consider the case in which Sb_2Te_3- and Sb_8Te_3-phases precipitate inside $AgSbTe_2$-matrix, similar DFT transport coefficient calculations are performed for both phases, as well. In

this context, the molar formation energies of both phases and the free energies of their interfaces with $AgSbTe_2$-matrix are simulated to predict their thermal stability and nucleation sequence.

5. Additionally, to address the influence of deviations from $AgSbTe_2$-stoichiometry on electron transport properties, the latter is simulated for two off-stoichiometric model alloys Ag_3SbTe_4 and $AgSb_3Te_4$.

Experimental procedures are divided into the following steps:

1. Model ternary ($AgSbTe_2$) and quaternary (3 at.% La-$AgSbTe_2$) alloys are synthesized by vacuum melting followed by quenching and hot-pressing. The appropriate conditions enabling formation of $AgSbTe_2$-matrix that dissolves La-atoms with no La-rich precipitates are found.
2. Differential scanning calorimetry (DSC) tests are implemented for both La-free and La-doped alloys to address thermal stability issues and how they are influenced by La-additions.
3. Temperature-dependent thermal conductivity of both alloys is determined to realize effects of La-doping and to compare them with those predicted from first-principles.
4. Similarly, both temperature-dependent electrical conductivity and Seebeck coefficients are measured for ternary and quaternary alloys to realize effects of La-doping and to compare them with those predicted from first-principles.
5. Finally, to assess whether La-doping contributes to conversion efficiency, TE power factor and figure-of-merit are evaluated for La-free and La-doped materials.

3. Research methods

This section provides a brief description of computational and experimental methods applied in this research.

3.1. First-principles calculation

The primary calculations are performed for $AgSbTe_2$ stoichiometric phase. To address, however, both optional cases of second-phase nucleation and deviations from stoichiometric composition, as described in Section 2, the following phases are simulated, as well: Sb_2Te_3, Sb_8Te_3, Ag_3SbTe_4, and $AgSb_3Te_4$.

3.1.1. The base $AgSbTe_2$ phase—structural and vibrational calculations

Silver-antimony-telluride of $AgSbTe_2$ stoichiometry is commonly known to introduce a cubic lattice structure; however, it was suggested, that it may coexist with tetragonal and rhombohedral forms [59]. The following optional space group symmetries: cubic (Pm-3m, No. 221),

http://dx.doi.org/10.5772/66086

tetragonal (P4/mmm, No. 123), and rhombohedral (R-3m, No. 166) have been simulated from first-principles [57]. Calculations of temperature-dependent Helmholtz free energy for these three polymorphs indicate that P4/mmm polymorph is the most stable one at temperatures above 400 K, whose energy exhibits close proximity to that of Pm-3m polymorph. Based on calculated v-DOS function for P4/mmm model alloy consisting of 4 atoms per simulation cell, **Figure 1a**, it was decided to test effects of doping with lanthanum atoms (to be discussed further below). To represent effects of La-doping with effective concentration of La atoms, that is close to realistic doping levels, a model compound of $Ag_7LaSb_8Te_{16}$ stoichiometry was constructed having the same P4/mmm space group symmetry as of the original $AgSbTe_2$ lattice. In this compound, consisting of 32 atoms per simulation cell, **Figure 1b**, La-atom substitutes for $^1/_8$ of Ag-atoms, so that, the resulting concentration is 3.125 at.% La. Computational parameters concerning structural relaxation and vibrational properties are provided in detail [57]. The effects of La-doping on vibrational and thermal properties will be discussed further below.

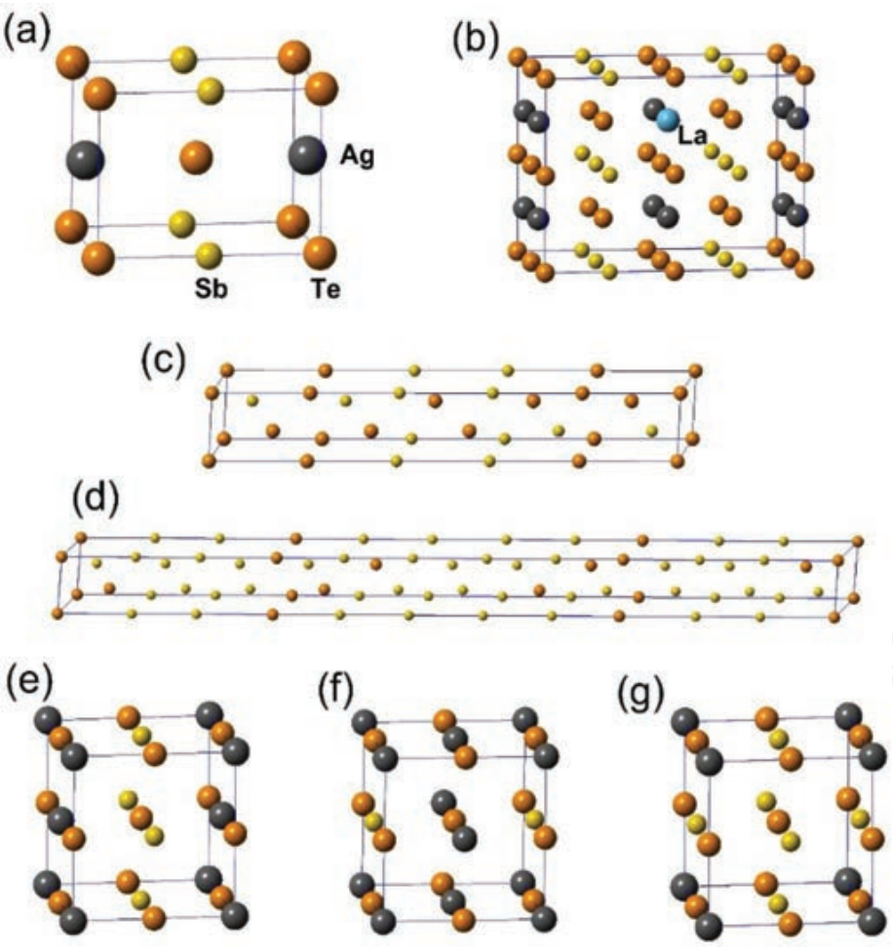

Figure 1. The lattice structures of model alloys discussed in this study and their space group symmetries: (a) $AgSbTe_2$ (P4/mmm); (b) $Ag_7LaSb_8Te_{16}$ (P4/mmm); (c) Sb_2Te_3 (R-3m); (d) Sb_8Te_3 (R-3m); (e) $(AgSbTe_2)_2$ (cubic P1); (f) Ag_3SbTe_4 (cubic P1); and (g) $AgSb_3Te_4$ (cubic P1).

3.1.2. The base $AgSbTe_2$ phase—electronic calculations

To simulate the effects of La-doping on electrical conductivity and Seebeck coefficient, electronic band structures are calculated for both lattices from first principles. A plane-wave basis set is implemented in Vienna *ab-initio* simulation package (VASP) [60–62] and *MedeA*® software environment [63]. The exchange-correlation electronic energy is expressed by means of generalized gradient approximation (GGA) using PBEsol energy functional [64] and projector augmented wave (PAW) potentials, which are utilized to represent core electron density [65]. Sampling of Brillouin zone is carried out using a set of uniform Monkhorst-Pack *k*-point mesh with density ranges between 0.14 and 0.17 $Å^{-1}$ and smearing method of linear-tetrahedron with Blöchl corrections [66]. To represent Kohn-Sham electronic wave functions, the plane waves are spanned with 400 eV energy cutoff for the structural relaxation or electronic calculations, respectively. Electronic optimization procedures are performed applying 10^{-5} eV energy convergence threshold.

The calculated 0 K band structures are used for evaluation of temperature-dependent electrical conductivity, electronic component of thermal conductivity, and Seebeck coefficient, applying near-equilibrium Boltzmann transport theory with constant relaxation time approximation, as implemented in BoltzTrap code [67].

The partial electrical conductivity tensor, $\sigma'_{\alpha\beta}(i, \mathbf{k})$, represented for *i*th energy band and a given **k**-point, is obtained from Cartesian component of electron group velocity by derivation of *i*th energy band, $\varepsilon_{i,k}$, with respect to α- and β-components of electron's wave vector [68]. $\sigma'_{\alpha\beta}(i, \mathbf{k})$ is then given by:

$$\sigma'_{\alpha\beta}(i, \mathbf{k}) = e^2 \tau_{i,k} \frac{1}{\hbar^2} \frac{\partial^2 \varepsilon_{i,k}}{\partial k_\alpha \partial k_\beta} , \tag{1}$$

where *e* is electron unit charge, $\hbar$ is reduced Planck constant, and $\tau_{i,k}$ is electron relaxation time, which is assumed to be constant. This yields temperature and chemical potential, μ, dependent electrical conductivity tensor with respect to α- and β-components, summed over N-energy bands:

$$\sigma_{\alpha\beta}(T, \mu) = \frac{1}{\Omega} \sum_{i=1}^{N} \int \sigma'_{\alpha\beta}(\varepsilon_i) \left[-\frac{\partial f_0(T, \varepsilon, \mu)}{\partial \varepsilon} \right] \mathrm{d}\, \varepsilon_i , \tag{2}$$

where Ω is characteristic unit cell volume and $f_0(T, \varepsilon, \mu)$ is equilibrium Fermi-Dirac distribution function [69]. The electronic component of thermal conductivity tensor, κ^e, is, accordingly, expressed by:

$$\kappa^e_{\alpha\beta}(T, \mu) = \frac{1}{e^2 T \Omega} \sum_{i=1}^{N} \int \sigma'_{\alpha\beta}(\varepsilon_i) \cdot (\varepsilon_i - \mu)^2 \left[-\frac{\partial f_0(T, \varepsilon, \mu)}{\partial \varepsilon} \right] \mathrm{d}\, \varepsilon_i . \tag{3}$$

Finally, the explicit expression for Seebeck coefficient tensor, S_{ij}, is given by [70, 71]:

$$S_{ij}(T, \mu) = [\sigma]^{-1}_{\alpha i} \frac{1}{eT\Omega} \sum_{i=1}^{N} \int \sigma'_{j\alpha}(\varepsilon_i) \cdot (\varepsilon_i - \mu) \left[-\frac{\partial f_0(T, \varepsilon, \mu)}{\partial \varepsilon} \right] \mathrm{d}\, \varepsilon_i . \tag{4}$$

http://dx.doi.org/10.5772/66086

3.1.3. The Sb_2Te_3 and Sb_8Te_3 phases

Nonmagnetic DFT calculations are performed for Sb_2Te_3 and Sb_8Te_3 crystal structures having (R-3m) space group symmetry, which incorporate 15 and 33 atoms per simulation cell, respectively. Both lattice structures are rendered in **Figure 1c** and **d**, respectively. A computational routine similar to aforementioned one is implemented with several differences. GGA approximation is applied for a set of uniform 9 × 9 × 9 Monkhorst-Pack *k*-point mesh, and plane waves are spanned with either 400 or 350 eV energy cutoff for structural relaxation or electronic calculations, respectively. Electronic optimization procedures are performed applying 10^{-6} eV energy convergence threshold.

Structural relaxation procedures are first performed, allowing variation of cell volume and atom positions at all degrees of freedom, setting a convergence threshold of 10^{-4} eV Å^{-1} for Hellman-Feynman forces. The resulting lattice parameters obtained for relaxed crystal structures are: a = b = 4.34 Å and c = 31.21 Å for Sb_2Te_3; and: a = b = 4.37 Å and c = 64.93 Å for Sb_8Te_3, which are in good agreement with data reported in the literature [72, 73]. Then, electronic band structure calculations are performed for both relaxed structures.

Band structures are calculated in the same manner as mentioned above, allowing calculations of temperature-dependent electrical conductivity, electronic component of thermal conductivity, and Seebeck coefficient values. These calculations yield p-type behavior for both structures, and we fine-tune the positions of electronic chemical potential to reside at the top of the valence bands. This yields Seebeck coefficient values that are very similar to those measured by us experimentally for pure Sb_2Te_3 standard. Additionally, we set electron relaxation time to be 8 fs, so as to fit electrical conductivity values calculated for Sb_2Te_3 with those measured for the same standards. We, then, apply the same relaxation time for Sb_8Te_3, as well.

To address bulk and interfacial energetic aspects related with nucleation of Sb_2Te_3 and Sb_8Te_3 phases in $AgSbTe_2$ phase, we have simulated formation energies of Sb_2Te_3 and Sb_8Te_3 phases and their interfaces with $AgSbTe_2$ phase. Molar formation energy of model Sb_pTe_q cell, $\underline{E}^{tot}_{Sb_pTe_q}$, is calculated using the following expression [57]:

$$\underline{E}^{f}_{Sb_pTe_q} = \frac{\underline{E}^{tot}_{Sb_pTe_q} - p \times \mu^{o}_{Sb} - q \times \mu^{o}_{Te}}{p+q}, \tag{5}$$

where $\underline{E}^{tot}_{Sb_pTe_q}$ is cell's molar total energy and μ^{o}_{Sb} and μ^{o}_{Te} are chemical potentials of Sb- and Te-atoms in their standard states, which are evaluated to be −397.72 and −303.12 kJ mol^{-1}, respectively. The free energy of silver-antimony-telluride (AST)/antimony-telluride (SBT) interface is calculated constructing a slab model having AST/SBT generic form, and using the following expression [74]:

$$\gamma = \frac{1}{2A}\left(E^{f}_{AST/SBT} - n_{AST}\,\underline{E}^{f}_{AST} - n_{SBT}\,\underline{E}^{f}_{SBT}\right), \tag{6}$$

where A is AST/SBT interface cross-sectional area, $E^{f}_{AST/SBT}$ is calculated formation energy of slab model, $\underline{E}^{f}_{AST}$ and $\underline{E}^{f}_{SBT}$ are calculated molar formation energies of AST and SBT sub-cells, and n_{AST} and n_{SBT} are their number of moles in the entire model slab, respectively.

3.1.4. Ag_3SbTe_4 and $AgSb_3Te_4$ model compounds

To simulate the effects of deviations from stoichiometric $AgSbTe_2$ composition, we construct three model alloys based on P4/mmm space group symmetry, which is reduced to cubic P1 symmetry, by setting equal lattice parameter of a = 6.113 Å for all. The resulting structures simulated are: $(AgSbTe_2)_2$, Ag_3SbTe_4, and $AgSb_3Te_4$, which appear in **Figure 1e, f,** and **g,** respectively. All three structures contain 8 atoms per unit cell and Sb/Ag ratios of 1, 1/3, and 3, respectively. To calculate band structures of these three model alloys, spin-orbit (SO) magnetic calculations were performed utilizing a similar GGA/PAW routine as described above for uniform 7 × 7 × 7 Monkhorst-Pack *k*-point mesh and 400 eV energy cutoff to represent Kohn-Sham electronic wave functions, applying 10^{-6} eV energy convergence threshold. SO coupling is often being considered in band structure calculations [32, 70, 75]. TE transport properties were calculated according to the procedure detailed by Eqs. (1)–(4).

3.2. Experimental procedure

3.2.1. Materials synthesis

Experimental procedures implemented in this study are intended to validate the effects of La-alloying on TE performance, as predicted from first principles. They include synthesis of two model alloys, La-free and La-alloyed, having molar ratios (Ag:Sb:Te:La) of 18:29:53:0 and 15.75:29:53:2.25, respectively. Generally, synthesis procedures comprise vacuum melting and iced-water quenching, followed by uniaxial hot-pressing at two distinct temperatures, 540 and 500°C, yielding two series of 12.7 mm dia. pellets referenced below as Series A and Series B, respectively. The difference between these two series of alloys is manifested by their phase contents and average composition in matrix. These factors significantly affect TE performance, as will be discussed further below. A detailed description of the experimental procedures appears elsewhere [58].

3.2.2. Materials and thermoelectric property characterization

Materials characterization procedures include microstructure, phase identification, and composition analysis employing scanning electron microscopy and X-ray diffraction [58]. Assessment of alloys' thermal stability is investigated using SETARAM 1600 DSC with a scanning rate of 25 K min^{-1} at temperatures ranging from room temperature through 973 K.

Temperature-dependent electrical conductivity, σ(T), and Seebeck coefficient, S(T) (thermopower), of these pellets are measured in temperature range from 300 to ~700 K employing *Nemesis*® SBA-458 apparatus (Netzsch GmbH), which is designed for simultaneous measurements of electrical conductivity and thermopower for planar geometry [76–78].

MicroFlash® LFA-457 laser flash analyzer (LFA; Netzsch GmbH) is utilized to measure directly of thermal diffusivity, α(T), of pellets in the same temperature range applying pulse-corrected Cowan approximation to consider heat loss of the samples [79], yielding instrumental accuracy of 2%. Material's density, ρ, is measured at room temperature, and density's dependence on temperature is neglected. Temperature-dependent heat capacity, C_p(T), is simultaneously

http://dx.doi.org/10.5772/66086

measured in LFA by comparative method using pure Al_2O_3—reference sample having similar geometry [76]. The resulting accuracy of evaluation of thermal conductivity values is equal to 10%. Pellets' thermal conductivity values, κ, are then determined by measuring their temperature-dependent thermal diffusivity and heat capacity, as well as, density; κ is then expressed by [80]:

$$\kappa(T) = \alpha(T) \cdot \rho \cdot C_p(T) . \quad (7)$$

4. Effects of La-alloying on thermoelectric performance

In this section, we introduce the concept resting behind La-alloying: its origin and implications, predictions from first principles, and experimental validations. Comparative discussion of the results in view of TE performance is provided.

4.1. Predictions from first-principles

4.1.1. The $AgSbTe_2$(P4/mmm) phase

4.1.1.1. Structural and vibrational properties

P4/mmm form of $AgSbTe_2$ phase is found to be the most stable one compared to all three polymorphs at temperatures larger than 400 K and exhibits Helmholtz free energy values with close proximity to those of cubic polymorph [57]. Frequency-dependent v-DOS, $g_p(\omega)$, calculated for this compound applying Debye approximation exhibits two major peaks at ca. 2.0 and 2.7 THz, and discloses interesting feature. Whereas, 2.7 THz peak comprises equal contributions from lattice vibrations of all sublattice sites, 2.0 THz one is primarily ascribed to vibrations of Ag-sublattice site atoms [57, 58]. This opens up the option of tuning v-DOS pattern by introducing point defects, a discipline for which the term *phonon engineering* has been coined [35]. Particularly, substitutions for Ag-sublattice sites by elements of different mass or atomic radius are expected to modify v-DOS with respect to that of pure $AgSbTe_2$ phase by suppressing its major v-DOS peak. This, consequently, will reduce lattice thermal conductivity. La has been suggested as optional substitution atom due to its relatively large mass and atomic radius compared to average values of $AgSbTe_2$, that is, 138.91 a.m.u. and 187 pm vs. 121.21 a.m.u. and 143.98 pm, respectively, giving rise to enhanced phonon scattering by point defects [81–84]. Furthermore, La-alloying has commercial outcomes, since La is the most inexpensive element compared to constituents of $AgSbTe_2$ alloy and is one of the less inexpensive ones among *energy-critical elements* [85].

Three substitutional options were tested, in which La substitutes for Ag, Sb, or Te, and it was found that substitution at Ag-sublattice sites is the most energetically preferred state for P4/mmm symmetry [57]. Accordingly, La-doped structure was constructed, in which one La-atom substitutes for 1/8. of Ag-atoms, and is shown in **Figure 1b**. First, v-DOS was calculated for La-doped structure and 2.0 THz peak was suppressed, as expected. Second, phonon dispersion curves were calculated for both $AgSbTe_2$ and $LaAg_7Sb_8Te_{16}$ alloys close to

Γ-point along c-crystallographic direction, indicating, that the slopes of the one longitudinal and two transverse acoustic modes of $AgSbTe_2$-lattice are greater, than those of La-alloyed one [57]. Quantitatively, average sound velocities derived for pure and La-alloyed materials are 1727 and 1046 m s^{-1}, respectively. Moreover, temperature-dependent heat capacity functions were determined for both structures, yielding slightly lower values for La-alloyed material. Both values of sound velocity and heat capacity that are found to decrease due to La-alloying imply, that La-alloying should reduce lattice thermal conductivity [57]. Additional calculations employing Debye approximation for low-temperature range of heat capacity yield Debye temperatures and sound velocities for both pure and La-alloyed materials, which are 112 K and 1684 m s^{-1} vs. 104 K and 1563 m s^{-1}, respectively [58]. It is noteworthy that evaluation of sound velocity in this manner is considered to be more physically reliable, since it represents the entire space of lattice directions, rather than individual one. It is, therefore, expected that this way of calculation should yield thermal conductivity values, that fit experimental data better than the former way does.

4.1.1.2. Effects of La-doping on thermal conductivity

Average sound velocity, v_s, and Debye temperature, θ_D, evaluated from first-principles serve as input, that is required to evaluate lattice thermal conductivity, κ_p. To this end, one possibility is to employ Callaway model for lattice thermal conductivity [86, 87], which has become conventional, particularly in the field of TE materials [36–38, 88–93]. In present case, however, there is no need to employ Callaway model for several reasons. First, Callaway model is specified for low temperatures, where contributions of either Normal (N)- or Umklapp (U)-processes are at the same order of magnitude. For temperatures adequately higher than Debye temperature (e.g., $\theta_D \approx 112$ K for $AgSbTe_2$ alloy) [30, 57], only U-processes dominate. Second, Callaway model considers $g_p(\omega)$ and $C_p(T)$ functions that are simplistically approximated based on Debye model [94]. In present case, however, the explicit $g_p(\omega)$ and $C_p(T)$ functions have already been calculated for both pure and La-alloyed materials. Alternatively, the following expression for lattice thermal conductivity is employed [94–96]:

$$\kappa_p = \frac{1}{3} C_v v_s^2 \tau , \tag{8}$$

where τ is phonon relaxation time. To first approximation, it has been assumed that La-doping influences mostly sound velocity and heat capacity and has negligible effect on τ. The ratio of $C_v v_s^2$-products obtained for $LaAg_7Sb_8Te_{16}$ and$AgSbTe_2$ alloys, therefore, reflects the lower limit of relative reduction in thermal conductivity due to La-alloying. Applying dispersion curves close to Γ-point along c-crystallographic direction, it is predicted, that κ_p should decrease by factor of ca. 2.7 due to La-doping. Alternatively, applying sound velocity values derived from Debye approximation, κ_p is expected to decrease by ca. 14% at room temperature due to La-doping [58].

A more thorough and accurate treatment of expression (8) considers the effects of La-alloying on τ, as well. To evaluate τ, contributions of two major scattering mechanisms are taken into account. The first one is phonon-phonon inelastic interactions, i.e., U-processes, that prevail

http://dx.doi.org/10.5772/66086

for these alloys above room temperature. Relaxation time for U-processes, τ_U, is represented by [96, 97]:

$$\tau_U^{-1} \approx \frac{\hbar \gamma^2}{M v_s^{\,2} \theta_D} \omega^2 T e^{\left(-\frac{\theta_D}{3T}\right)}, \tag{9}$$

where γ is Grüneisen parameter that reflects the degree of lattice anharmonicity [69], and M is average atomic mass of alloy. Second, to account for internal composition inhomogeneity or compositional modulations at unit-cell length scales, that are typical for such materials [5, 8, 16, 91], the boundary scattering mechanism is employed for characteristic period l, represented by relaxation time τ_B, so that [96]:

$$\tau_B^{-1} \approx \frac{v_s}{l}. \tag{10}$$

To consider dependence of v-DOS on phonon frequency, frequency-averaged expression for τ_U is introduced, so that $g_p(\omega)$ serves as weighting function:

$$\langle \tau_U^{-1} \rangle_\omega = \frac{\hbar \gamma^2}{M v_s^{\,2} \theta_D \omega_D} T e^{\left(-\frac{\theta_D}{3T}\right)} \int_0^{\omega_D} \omega^2 g_p(\omega) d\omega, \tag{11}$$

where ω_D is Debye frequency. Equivalent relaxation time is then expressed as:

$$\tau^{-1} = \langle \tau_U^{-1} \rangle_\omega + \tau_B^{-1}. \tag{12}$$

The resulting values of lattice thermal conductivity for $LaAg_7Sb_8Te_{16}$ and $AgSbTe_2$ alloys are obtained from Eq. (8) by substituting the respective physical magnitudes for both alloys in Eqs. (9)–(11) [19, 20, 30, 57, 58, 92] with $l \approx 1$ nm [5, 8, 16, 91]. Lattice thermal conductivity for $LaAg_7Sb_8Te_{16}$ and $AgSbTe_2$ alloys calculated as function of temperature appear in **Figure 2**.

It is shown that thermal conductivity exhibits realistic values, that correspond with data documented in the literature [19, 20, 25, 98] with marked decrease due to La-doping, ranging between relative values of 11 and 19%, depending on temperature.

4.1.1.3. Effects of La-doping on electrical properties

It was shown that La-alloying reduces lattice thermal conductivity values, which affects TE performance positively. To address, however, the total effects of La-alloying on TE performance, evaluation of electrical conductivity and Seebeck coefficient is essential. This goal was achieved from first-principles applying Boltzmann transport theory as described above for $LaAg_7Sb_8Te_{16}$ and $AgSbTe_2$ alloys. The results are plotted in **Figure 3** in temperature range 50–1000 K.

It is found that La-doping results in reduction in electrical conductivity (e.g., from ca. 1800 down to 250 S cm^{-1} at room temperature) and, at the same time, increase in Seebeck coefficient, e.g., from ca. 4 up to 40 μV K^{-1} at room temperature. For the sake of comparison, Jovovic

and Heremans reported on experimental measurements of electrical conductivity and Seebeck coefficients of stoichiometric and doped $AgSbTe_2$ alloys at temperatures up to 400 K [19, 98]. For example, they report on electrical resistivity value of 5×10^{-5} Ohm m at 100 K for stoichiometric $AgSbTe_2$ alloy, which is equivalent to 200 S cm^{-1}.

They report also on electrical resistivity that increases with temperature, indicating charge carriers scattering. Additionally, electrical resistivity may either increase or decrease with doping, depending on dopant's chemical identity. In the present case, electrical conductivity values are significantly larger, e.g., ca. 1900 S cm^{-1} at 100 K, and are decreasing with temperature, where La-doping reduces conductivity. Seebeck coefficient values reported by Jovovic et al. exhibit general trend of increase with temperature, which corresponds to trend calculated in the present case. Also, they report on general trend of increase in Seebeck coefficient values due to doping (except doping with AgTe), in agreement with the present study for La. Complementary trend is reported by Du et al. [25, 99]. Most interestingly, effects of La-doping on electrical properties of $AgSbTe_2$ alloy are reported by Min et al. [27]. They report on trends that are qualitatively similar to those of the present study. First, La-doping was also reported to reduce electrical conductivity, e.g., from ca. 400 S cm^{-1} for undoped $AgSbTe_2$ down to 66 S cm^{-1} for 3 at.% La-doping at room temperature. Second, La-doping increases Seebeck coefficients, e.g., from ca. 90 $\mu V \cdot K^{-1}$ for undoped $AgSbTe_2$ up to ca. 220 μV K^{-1} for 3 at.% La-doping at room temperature. Quantitatively, values of electrical conductivity calculated in this study are considered to be large with respect to the above cited studies. Conversely, Seebeck coefficient values calculated in this study are considered to be smaller than those reported by the above studies. We note, however, that such calculations are most meaningful for comparative purposes, since they rest upon values, that should be calibrated against experimental data, such as electronic chemical potential and relaxation times.

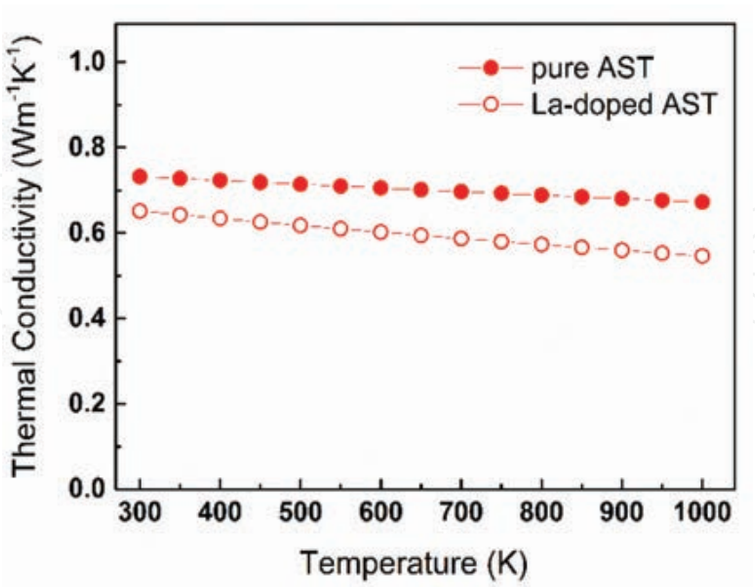

Figure 2. The lattice thermal conductivity values calculated from first-principles for $AgSbTe_2$ (pure AST; filled red circles) and $LaAg_7Sb_8Te_{16}$ (La-doped AST; empty red circles) alloys in temperature range 300–1000 K.

http://dx.doi.org/10.5772/66086

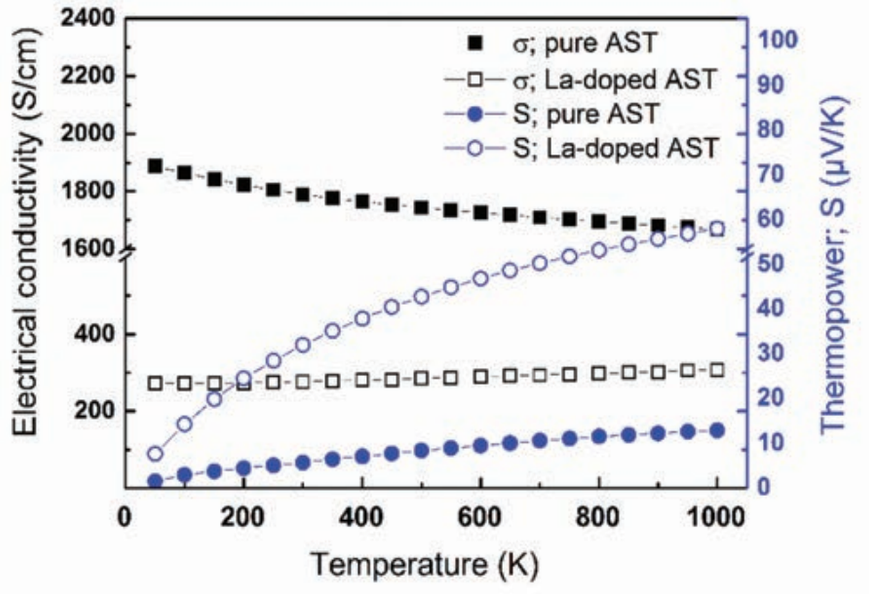

Figure 3. Electrical conductivity and Seebeck coefficient values calculated for $AgSbTe_2$ (pure AST; filled black squares and blue circles, respectively) and $LaAg_7Sb_8Te_{16}$ (La-doped AST; empty black squares and blue circles, respectively) alloys in temperature range 50–1000 K from first-principles applying Boltzmann transport theory.

It is indicated that the effects of La-doping on electrical conductivity and Seebeck coefficient are opposite to each other. Evaluation of TE power factor (PF; $S^2\sigma$) is, therefore, necessary in order to realize how La affects TE power conversion. **Figure 4** displays PF calculated for $LaAg_7Sb_8Te_{16}$ and $AgSbTe_2$ alloys in temperature range 50–1000 K.

It is shown that La-doping has considerably positive effect on PF. This also corresponds with the data reported by Min et al. [27], specifically for low La-concentration regime. We note that, moreover, La-doping reduces lattice thermal conductivity, as shown in **Figure 2**. We conclude that La-alloying should improve energy conversion efficiency of $AgSbTe_2$ (P4/mmm), as reflected by increased TE figure-of-merit.

4.1.2. Formation of Sb_2Te_3 and Sb_8Te_3(R-3m) phases

The single δ-phase is Sb-rich phase based on $AgSbTe_2$ alloy. Since it has limited solubility to Sb with relatively moderate slope of Sb-solvus, it is likely to decompose to δ+Sb_2Te_3 phase mixture [28, 29, 100–103], whereas Sb_2Te_3 is equilibrium phase and may appear as different homologous forms [72, 73, 104–107]. Precipitation of antimony-telluride second phase in δ-matrix is expected to affect TE performance due to contributions from both matrix and precipitate phases or variation of the average matrix composition. In the following sections, we address both aspects. Section 4.1.2.1 introduces the issue of precipitation sequence based on bulk/interfacial energetic considerations, and Section 4.1.2.2 predicts the effects of phase formation on electronic properties. Then, Section 4.1.3 deals with compositional variations in the matrix and their effects on electronic properties.

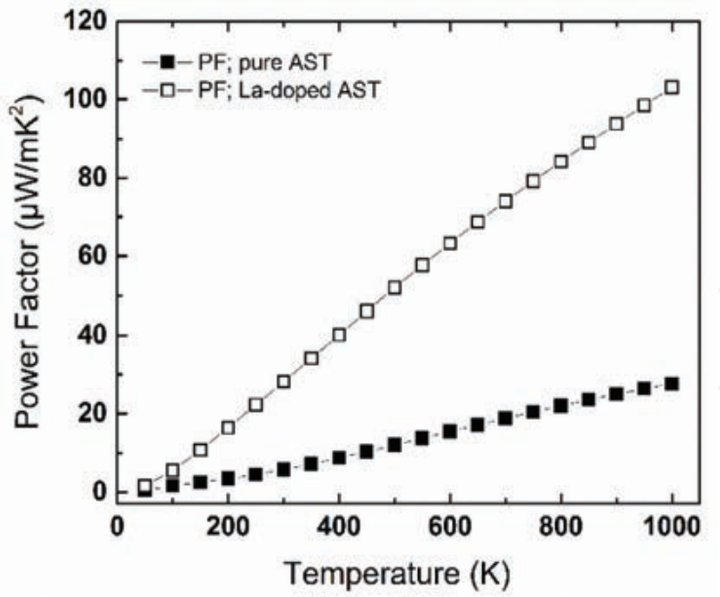

Figure 4. Thermoelectric power factor (PF) calculated for $AgSbTe_2$ (pure AST; filled black squares) and $LaAg_7Sb_8Te_{16}$ (La-doped AST; empty black squares) alloys in temperature range 50–1000 K from first-principles applying Boltzmann transport theory.

4.1.2.1. The precipitation sequence: energetic aspects

Nucleation of Sb_2Te_3 and Sb_8Te_3 phases from Sb-saturated δ-$AgSbTe_2$ matrix has been observed, which can be associated to different experimental conditions. To account for the sequence of phase formation, information on both bulk and interfacial energetics is required. The formation energies of Sb_2Te_3 and Sb_8Te_3 (R-3m) phases, calculated according to Eq. (5), are −62 and −56.6 kJ mol^{-1}, respectively. This implies that Sb_2Te_3 is more energetically favorable, assuming, that Sb_2Te_3 precipitates are adequately large, so that, interfaces do not play significant role. To address the role of interfaces, free energies of $Sb_2Te_3/AgSbTe_2$ and $Sb_8Te_3/AgSbTe_2$ interfaces are evaluated. To this end, two slab models of $(Sb_2Te_3)_2/(AgSbTe_2)_5/(Sb_2Te_3)_2$ (40 atoms) and $(AgSbTe_2)_3/(Sb_8Te_3)_6/(AgSbTe_2)_3$ (90 atoms) forms are constructed, respectively, consisting of two interfaces each, exhibiting $(111)_{AgSbTe_2} \parallel (0001)_{Sb_pTe_q}$ and $\langle 10\bar{1}\rangle_{AgSbTe_2} \parallel \langle \bar{2}110\rangle_{Sb_pTe_q}$ orientation relationship, which was observed experimentally [100]. Both structures are displayed in **Figure 5**.

It is noted that two interfaces presented in both slabs shown in **Figure 5a** and **b** consist of different Sb- and Te-terminating planes, so that interfacial free energies calculated according to Eq. (6) represent an average value for both terminations. Correction factor is, therefore, applied to represent interfacial free energy of low-energy Sb-termination. The resulting values for $Sb_2Te_3/AgSbTe_2$ and $Sb_8Te_3/AgSbTe_2$ interfaces are $\gamma = 208$ and 175 mJ m^{-2}, respectively. These values are considered to be relatively low compared to those of intermetallic compounds and are comparable with those of pure metals [108]. This is, however, not surprising, considering the extremely small atomic misfit between the $(111)_{AgSbTe_2}$ and $(0001)_{Sb_pTe_q}$ crystallographic planes [100], which encourages formation of Sb_2Te_3 or Sb_8Te_3 precipitates in the form of long lamellae along these planes [28, 29, 57, 58, 100–103]. These low values of interfacial free energy also initiate fast nucleation, thanks to low activation energy for nucleation, which is proportional to γ^3 [109].

http://dx.doi.org/10.5772/66086

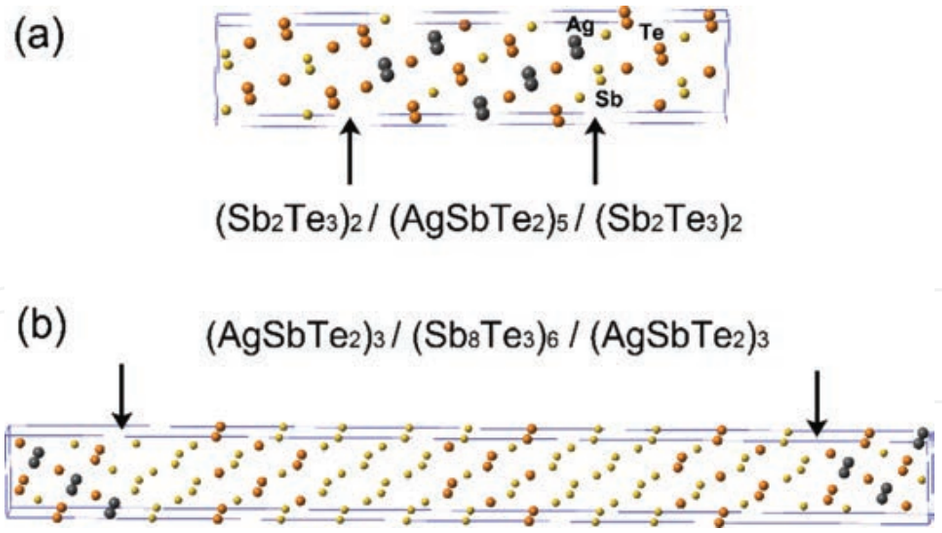

Figure 5. Two slab models of (a) $(Sb_2Te_3)_2/(AgSbTe_2)_5/(Sb_2Te_3)_2$ (40 atoms) and (b) $(AgSbTe_2)_3/(Sb_8Te_3)_6/(AgSbTe_2)_3$ (90 atoms) including two $Sb_2Te_3/AgSbTe_2$ and $Sb_8Te_3/AgSbTe_2$ interfaces each, respectively. All interfaces, marked by arrows, are of $(111)_{AgSbTe2} \parallel (0001)_{SbpTeq}$ and $\langle 10\bar{1}\rangle_{AgSbTe2} \parallel \langle \bar{2}110\rangle_{SbpTeq}$ orientation relationship.

Interestingly, Sb_2Te_3 phase exhibits lower value of formation energy and higher value of interfacial free energy compared to those of Sb_8Te_3 phase. This implies that Sb_8Te_3 is metastable phase that may form prior to the nucleation of Sb_2Te_3 equilibrium phase [28, 29, 100–103]. Suggested nucleation sequence is, therefore, supersaturated-δ → supersaturated-δ + Sb_8Te_3 → equilibrium-δ + Sb_2Te_3.

4.1.2.2. Effects of Sb_2Te_3 and Sb_8Te_3 formation on electronic properties

In view of aforementioned prospect for the presence of either of Sb_2Te_3- or Sb_8Te_3-phases in $AgSbTe_2$-matrix, calculations of transport coefficients of these phases provide us with predictions of the effects such phase mixture on TE performance. **Figure 6** displays electrical conductivity and Seebeck coefficients calculated in temperature range 50–1000 K.

It is shown that both electrical conductivity and Seebeck coefficient values of Sb_2Te_3 phase are larger than those of Sb_8Te_3 phase in wide temperature range, e.g., ca. 2100 S cm^{-1} and 85 μV K^{-1} for Sb_2Te_3 compared to 1380 S cm^{-1} and 29 μV K^{-1} for Sb_8Te_3 at 300 K, respectively. Moreover, comparison of these results with the data shown in **Figure 3** for $AgSbTe_2$-matrix implies that precipitation of Sb_2Te_3 phase yields positive influence on TE performance: both electrical conductivity and Seebeck coefficient increase. It is strikingly indicated that the effects of Sb_2Te_3 precipitation are even greater, than those of La-doping. It is, therefore, concluded that the desirable material from TE viewpoint is La-doped, Sb-supersaturated δ-$AgSbTe_2$-matrix that is aged for a certain duration to form considerable amount of Sb_2Te_3 phase. The effects of Sb_8Te_3 phase on TE performance are, conversely, inferior to those of Sb_2Te_3 phase. Sb_8Te_3 is, however, metastable phase and is not expected to prevail for long durations at elevated temperatures (e.g., under service conditions of TE generator) due to low thermal stability.

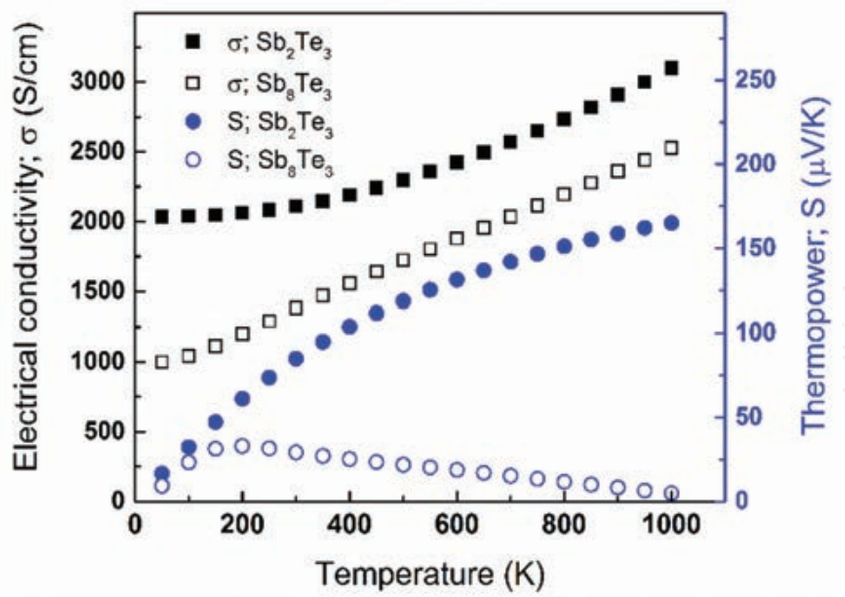

Figure 6. Electrical conductivity and Seebeck coefficient values calculated for Sb_2Te_3 (filled black squares and blue circles, respectively) and Sb_8Te_3 (empty black squares and blue circles, respectively) compounds in temperature range 50–1000 K from first-principles applying Boltzmann transport theory.

4.1.3. Effects of off-stoichiometry on electronic properties of the $AgSbTe_2$ phase

An additional effect taking place during precipitation of any Sb_pTe_q phase from Sb-supersaturated δ-matrix is enrichment of δ-matrix with Ag-atoms and depletion of Sb. To simulate these compositional variations, two off-stoichiometric model alloys are constructed, namely Ag_3SbTe_4 and $AgSb_3Te_4$, in addition to stoichiometric $AgSbTe_2$ phase. These model compounds, appearing in **Figure 1e, g,** and **f,** exhibit Sb/Ag ratios of 1/3, 3, and 1, respectively. **Figure 7** displays electrical conductivity and Seebeck coefficient values calculated in temperature range 50–1000 K.

It is shown, that increase in Sb/Ag ratio results in decrease in electrical conductivity simultaneously with increase in Seebeck coefficient. This trend corresponds well with study of Jovovic and Heremans [19], who reported on decrease in both Seebeck coefficient and electrical resistivity due to additions of 2% AgTe to stoichiometric $AgSbTe_2$-phase, i.e., reducing Sb/Ag ratio. It should be noted that comparison of this trend with data reported in the literature is not straightforward, since compositional changes involve in practice not only Sb/Ag ratio, but also ratio of Te to any of the other species. Additionally, deviations from given stoichiometry often involve formation of second phases, which is not directly simulated here. For instance, Zhang et al. reported on dependence of TE properties on composition for $Ag_{2-y}Sb_yTe_{1+y}$-based alloys and found that electrical conductivity increases, while Seebeck coefficient decreases with *y*-values increasing from 1.26 up to 1.38 [101].

Most importantly, this predicted effect of Sb/Ag ratio on electrical properties has major implications on the temporal evolution of TE performance of the material during aging heat treatments (below Sb-solvus), or of TE generator during service. Since Sb_pTe_q phases nucleate from Sb-supersaturated δ-matrix during heat treatments, Sb/Ag ratio in δ-matrix decreases. This

http://dx.doi.org/10.5772/66086

should be accompanied by increase in electrical conductivity concurrently with decrease in Seebeck coefficient.

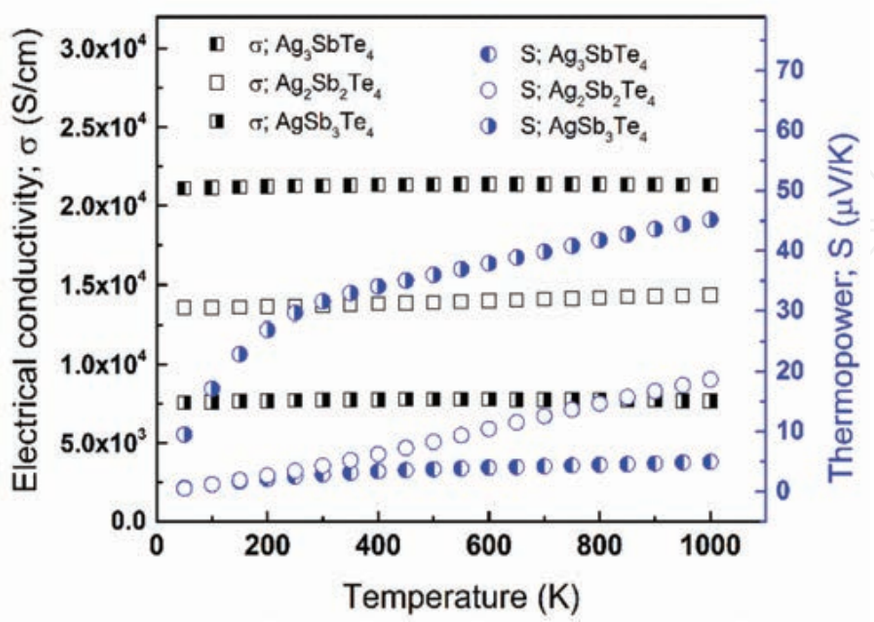

Figure 7. Electrical conductivity and Seebeck coefficient values calculated for Ag_3SbTe_4 (left-half-filled black squares and blue circles, respectively), $(AgSbTe_2)_2$ (empty black squares and blue circles, respectively), and $AgSb_3Te_4$ (right-half-filled black squares and blue circles, respectively) alloys in temperature range 50–1000 K from first-principles applying Boltzmann transport theory.

5. Experimental results

It was shown above how first-principles calculations provide us with information about all aspects concerning TE transport behavior, including thermal and electrical conductivity and Seebeck coefficient. Most importantly, this assists us in tailoring the material by introducing lattice defects to enhance its TE performance. In the following section, we introduce experimental procedures taken for validating the above predictions. Comparing between both aspects is, moreover, very instructive not only on engineering aspects, but also on universal aspect, by realizing how to implement computational tools to predict properties of other materials.

5.1. Microstructure and implications on thermoelectric behavior

As mentioned above, two classes of La-alloyed $AgSbTe_2$-based materials were prepared by uniaxial hot-pressing at 540 or 500°C, and are classified as Series A and Series B, respectively. The ideal case for testing the effects of La-doping is single δ-phase dissolving La homogeneously. This, however, is difficult to achieve. Hot-pressing at 540°C, that is, above Sb-solvus, expected to yield the desirable single δ-phase that does not contain Sb_2Te_3 precipitates [101–103]. These Sb_2Te_3 precipitates, indeed, were not observed in Series A samples; however, La-rich precipitates having stoichiometry close to $LaTe_2$ were observed [110]. As a result, δ-matrix was found

to be depleted of La [58], which does not allow us comparison between La-free and La-doped samples. Conversely, samples of Series B, that were hot-pressed at 500°C, exhibit considerable amount of Sb_2Te_3 phase, which is expected; however, $LaTe_2$ precipitates are dissolved, so that δ-matrix contains adequately large amount of La, close to its nominal concentration. Series B is, therefore, more suitable to exemplify the effects of La-doping. Moreover, as predicted from first-principles, the presence of Sb_2Te_3 precipitates, in addition to La solute atoms, has positive effects on electronic transport.

5.2. Thermal analysis

Thermal conductivity measurements performed for both Series A and Series B indicate the expected trend. First, all thermal conductivity values lie in the range 0.6–0.8 W m^{-1} K^{-1} [58]. Second, samples of Series A did not exhibit any considerable difference between La-free and La-doped materials [58]. This is associated to depletion of δ-matrix from La solute atoms, so that, matrix composition of La-doped and La-free materials is practically the same. Third, and most importantly, it was found that thermal conductivity of La-doped materials is significantly lower than those of La-free materials of Series B, e.g., 0.8 W m^{-1} K^{-1} for La-free and 0.6 W m^{-1} K^{-1} for La-doped samples at 500 K. This is strikingly corroborated by predictions from first-principles, both qualitatively and quantitatively, as shown in **Figure 2**. It is also noteworthy that both values coincide at temperatures larger than 650 K, which can be associated with phase transition [58, 101–103]. Thorough discussion of thermal conductivity values measured for Series A and Series B materials and their relationship with microstructure appears elsewhere [58]. To address this issue of phase transition, DSC measurements were implemented for both La-free and La-doped samples, **Figure 8**.

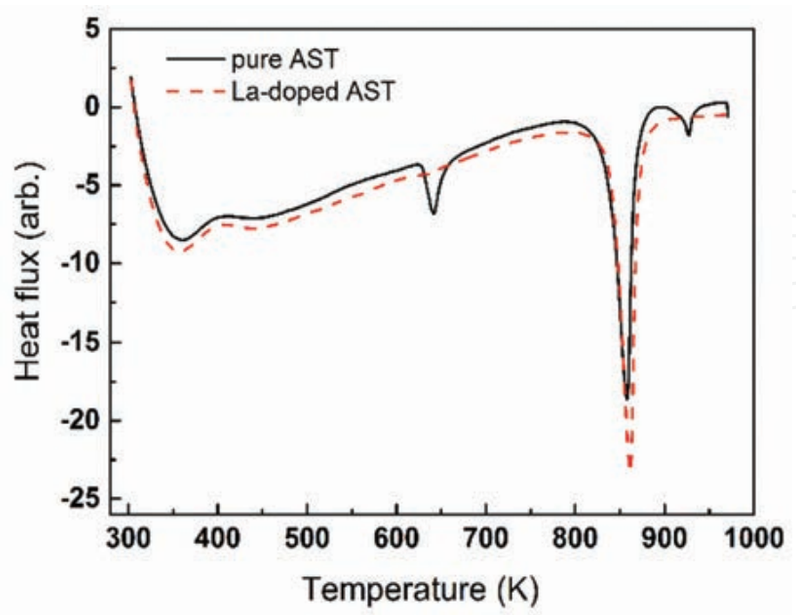

Figure 8. Differential scanning calorimetry (DSC) signals collected upon heating from La-free (continuous black curve) and La-doped (dashed red curve) samples.

http://dx.doi.org/10.5772/66086

Endothermic peak at around 630–650 K is observed for La-free material, which is associated with $Ag_2Te + Sb_2Te_3 \rightarrow \delta\text{-}AgSbTe_2$ phase transition at 360°C [101–103]. La-doped material, however, does not exhibit this transition. This corresponds well with thermal conductivity behavior reported by us earlier [58], in which temperature-dependent thermal conductivity of La-doped materials show up continuous trend, whereas La-free materials exhibit sharp drop of thermal conductivity around this temperature. This implies that La-additions help in stabilizing δ-phase against decomposition, which is expected to contribute to stability of TE device operation at service conditions. Sharp endothermic peak at ca. 860 K, which is common for both La-free and La-doped materials, is associated to melting.

5.3. Electrical property measurements

It was predicted from first-principles that La-doping reduces electrical conductivity and increases Seebeck coefficient, **Figure 3**. Measurements of electrical conductivity and Seebeck coefficients were carried out for both Series A and Series B materials. The samples of Series B are of our interest, since they dissolve La-atoms in δ-matrix; we will, therefore, introduce these results first. **Figure 9** displays experimentally collected electrical conductivity and Seebeck coefficient values of La-free and La-doped materials of Series B.

It is shown that electrical conductivity values decrease, e.g., from ca. 1400 down to 900 S cm^{-1} at room temperature, and Seebeck coefficient increase, e.g., from ca. 30 up to 70 μV K^{-1} at room temperature, due to La-doping. This behavior is, qualitatively, the same as that observed for calculated values shown in **Figure 3**. Moreover, temperature dependence, that is, electrical conductivity decreasing and Seebeck coefficient increasing with temperature for both La-free and La-doped materials, is identical to that indicated by calculated values shown in **Figure 3**. There are two major differences between experimental and calculated values appearing in **Figures 3** and **9**, respectively. First, the absolute values of measured Seebeck coefficient values are greater than calculated ones. Also, difference of electrical conductivity between La-doped and La-free materials is smaller for measured dataset than for calculated ones. This is probably due to difficulty to simulate low dopant concentrations in DFT [70]. Second, it is noteworthy that both values of electrical conductivity and Seebeck coefficients measured for La-free and La-doped materials converge at temperatures >650 K, **Figure 9**. Interestingly, these convergences occur due to sharp deviations of the values featured by La-free material, whereas the values of La-doped materials preserve their continuous trendline. This observation corresponds well with the behavior shown by DSC curves in **Figure 8**, where La-free compound decomposes at around 650 K, whereas La-doped compound seem to preserve its thermal stability. This also corresponds with converging thermal conductivities of the samples of Series B as discussed above [58]. Following our comparative discussion in Section 4.1.1.3, experimental values of electrical properties are found to be closer to experimental values reported in the literature than to calculated values [19, 25, 27, 98, 99].

To complement our understanding of the effects of La-doping on electronic properties, we measured temperature-dependent electrical conductivity and Seebeck coefficient values for the samples of Series A, as well. The results are plotted against temperature in **Figure 10**.

Comparison between the results attained for alloys of Series A and Series B is very instructive. As noted, the samples of Series A exhibited formation of $LaTe_2$-like precipitates, which "drain out" La atoms from δ-matrix, resulting in matrix compositions, that are nearly identical to each other for La-free and La-doped materials. For this reason, thermal conductivity values measured for La-free and La-doped materials seem to be practically identical in wide temperature range [58]. It is, therefore, not surprising to observe the same behavior for electrical properties, **Figure 10**.

It is indicated, that both electrical conductivity and Seebeck coefficient values measured for La-free and La-doped materials seem to be very close to each other in the entire temperature range, probably due to nearly identical matrix compositions for La-free and La-doped materials. Additionally, electrical conductivity and Seebeck coefficients featured by La-doped alloys exhibit relatively continuous temperature-dependent behavior, whereas values, measured for La-free alloys exhibit curled behavior. This, again, can be explained in terms of poor thermal stability of La-free materials, as discussed above.

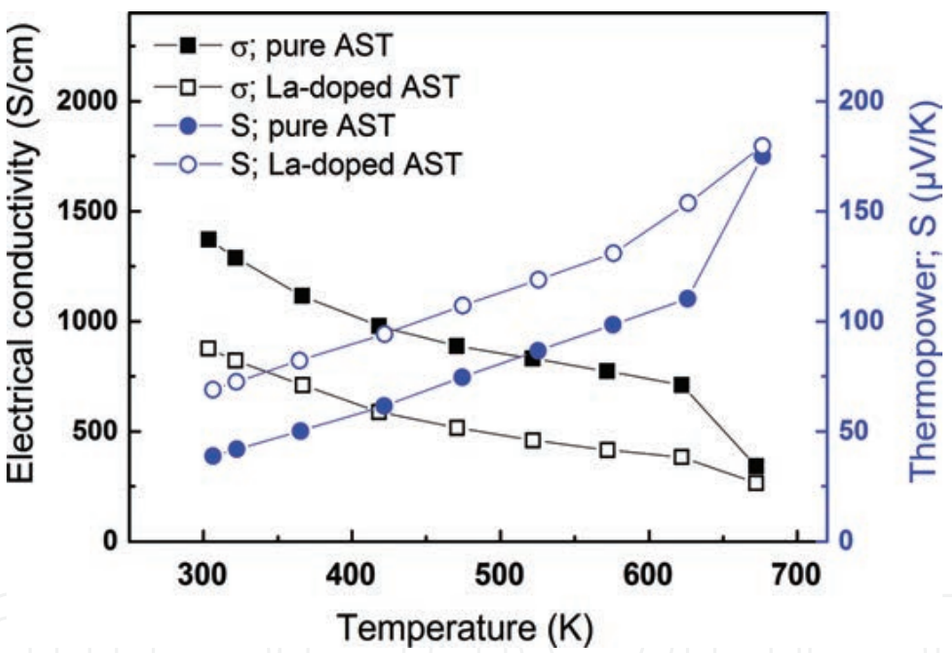

Figure 9. Electrical conductivity and Seebeck coefficient values measured for La-free (pure AST; filled black squares and blue circles, respectively) and La-doped (La-doped AST; empty black squares and blue circles, respectively) alloys of Series B in temperature range 300–673 K.

5.4. Implications for thermoelectric power conversion

It has been shown that La-doping has unequivocally positive effect on reducing lattice thermal conductivity, both computationally and experimentally. The effects on electrical properties, particularly electrical conductivity and Seebeck coefficient, are opposing each

http://dx.doi.org/10.5772/66086

other. To assess the effects of La-doping on device's power capacity, TE PFs of La-free and La-doped materials of Series B are evaluated based on the data displayed in **Figure 9**. The results are shown in **Figure 11**.

It is clearly shown that La-doping affects positively PF for temperatures lower than 500 K, e.g., PF determined for room temperature increases from ca. 200 to 400 μW m^{-1} K^{-2} due to La-doping. At higher temperatures, PFs of La-free and La-doped materials are practically identical. The maximum PF values observed are around 1000 μW m^{-1} K^{-2}. This trend is similar to that reported by Min et al. [27], that is, PF increasing from 300 up to 1500 μW m^{-1} K^{-2} in respective temperature range from room temperature to 400°C for $AgSbTe_2$ alloy.

La-doping was tested by them for different compositions, where composition yielding the greatest PF values is $AgSb_{0.99}La_{0.01}Te_2$, with PF values around 1000–1200 μW m^{-1} K^{-2} in the entire temperature range. Particularly, this La-doped material exhibits superior PF values up to ca. 325°C. This trend is similar to that reported by us in this study.

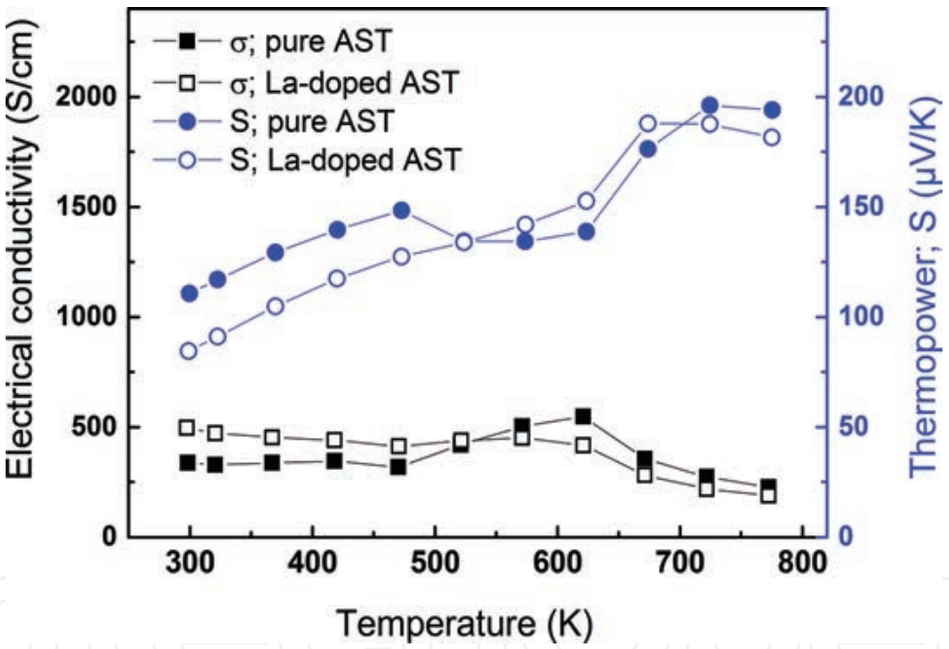

Figure 10. Electrical conductivity and Seebeck coefficient values measured for La-free (pure AST; filled black squares and blue circles, respectively) and La-doped (La-doped AST; empty black squares and blue circles, respectively) alloys of Series A in temperature range 300–773 K.

Finally, determination of TE figure-of-merit for both La-free and La-doped materials will provide us with the ultimate indication whether La-doping enhances TE power conversion efficiency. Based on thermal and electrical properties measured for Series A and Series B, temperature-dependent *ZT* values were determined and appear in **Figure 12**.

Most importantly, it is shown that La-doping increases *ZT* values markedly, **Figure 12b**, e.g., from ca. 0.3 to 0.45 at 473 K. This improvement is due to decrease in thermal conductivity in almost the entire temperature range and increase in PF at low-temperature regime due to La-doping. Above 600 K, again, both values of La-free and La-doped alloys converge due to poor thermal stability of La-free materials. *ZT* values of La-free and La-doped materials shown in **Figure 12b** correspond with those reported by Zhang et al. [101], where the effects of La-doping are comparable to those of stoichiometric variations about $AgSbTe_2$ composition. Similar values are reported by Mohanraman et al. [43] and Jovovic and Heremans [19] for Bi-doping, as well as, for Pb-doping [19]. Chen et al. obtain similar *ZT* values for Ge-doping [111] and for Sn-doping [112], depending on concentration. *ZT* values reported in the present study are, however, lower than those reported by Du et al. [25, 99], probably owing to different processing conditions yielding higher electrical conductivity values [113].

The picture, revealed for alloys of Series A, is, however, different; it is shown in **Figure 12a** that La-doping has little or no effect on *ZT*. This is, again, not surprising and follows the trends featured by Series A alloys for electrical conductivity and Seebeck coefficient, **Figure 9**, and thermal conductivity [58] associated to depletion of La-atoms from δ-matrix in La-alloyed materials hot-presses at 540°C.

Figure 11. Thermoelectric power factor (PF) values evaluated for La-free (pure AST; filled black squares) and La-doped (La-doped AST; empty black squares) alloys of Series B in temperature range 300–673 K.

http://dx.doi.org/10.5772/66086

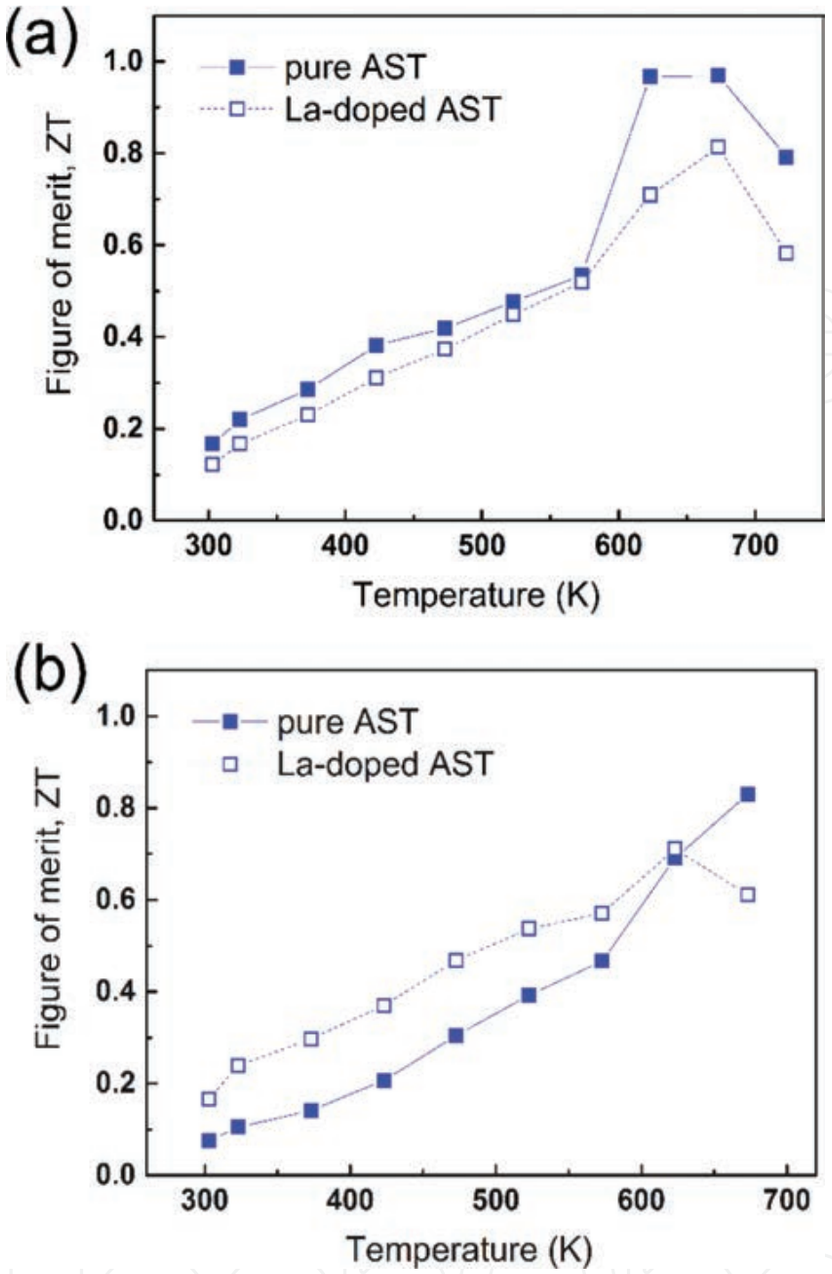

Figure 12. Thermoelectric figure of merit (ZT) values evaluated for La-free (pure AST; filled blue squares) and La-doped (La-doped AST; empty blue squares) alloys of (a) Series A and (b) Series B in temperature range 300–673 K.

6. Summary and concluding remarks

This chapter introduced the following findings. Computationally, total energy calculations for different polymorphs of $AgSbTe_2$ phase yield their Helmholtz free energies, implying, that P4/mmm space group symmetry is the most stable one at temperatures adequately higher than room temperatures. Predictions of the effects of doping on thermal conduc-

tivity are established on calculations of vibrational properties, such as phonon dispersion and density of states, from first-principles. Based on specific features in v-DOS curve, it is hypothesized that La-substitution for Ag-sites should result in reduced lattice thermal conductivity. These calculations predict reduction in average sound velocity from 1684 to 1563 m s^{-1} and of Debye temperature from 112 to 104 K due to La-doping. Applying Umklapp mechanism for phonon scattering with frequency-averaged inverse relaxation time, which is combined with boundary scattering, yields temperature-dependent functional forms for lattice thermal conductivity. Marked decrease due to La-doping, ranging between relative values of 11 and 19% depending on temperature, are observed. Then, calculations of electronic band structures of both La-free and La-doped lattices are performed, yielding TE transport coefficients applying Boltzmann transport theory. It is found that La-doping results in reduction in electrical conductivity (e.g., from ca. 1800 down to 250 S cm^{-1} at room temperature) at the same time with increase in Seebeck coefficient, e.g., from ca. 5 up to 40 μV K^{-1} at room temperature.

Attempts to infer conclusions with practical implications from DFT calculations must consider engineering aspects that extend further beyond single phase state having high symmetry unit cell, that maintains its physical properties with time. For example, considerations, such as long-term device operation under elevated service temperatures, should be taken into account. Such case requires original solution for simplified (or, sometimes, over-simplified) approach offered by DFT. Particularly, for the case of thermal stability, exposure of Sb-rich δ-phase to elevated temperatures results in precipitation of Sb_pTe_q-based phases at the same time with decrease in Sb/Ag ratio in δ-matrix. In this manner, thermal stability issues can be addressed by dividing the realistic conditions into a set of simplified problems, each can be handled by DFT. To this end, we first consider the case in which Sb_2Te_3 and Sb_8Te_3 phases precipitate inside $AgSbTe_2$-matrix. It is found that both electrical conductivity and Seebeck coefficient values of Sb_2Te_3-phase are larger, than those of Sb_8Te_3-phase in wide temperature range, e.g., ca. 2100 S cm^{-1} and 85 μV K^{-1} for Sb_2Te_3 compared to1380 S cm^{-1} and 29 μV K^{-1} for Sb_8Te_3 at 300 K, respectively. Moreover, it is estimated that precipitation of Sb_2Te_3-phase in $AgSbTe_2$-matrix is expected to improve the total values of both electrical conductivity and Seebeck coefficient. Concerning nucleation sequence of Sb_2Te_3 and Sb_8Te_3 phases in $AgSbTe_2$, their molar formation energies and interfacial free energies were calculated, suggesting that Sb_8Te_3 nucleates first as metastable phase, prior to the formation of equilibrium Sb_2Te_3 phase. Second, to address the influence of deviations from $AgSbTe_2$ stoichiometry on electron transport properties, off-stoichiometric model alloys Ag_3SbTe_4 and $AgSb_3Te_4$ were simulated. It is found that increase in Sb/Ag ratio results in decrease in electrical conductivity simultaneously with increase in Seebeck coefficient. Considering both effects of Sb_2Te_3 precipitation accompanied by simultaneous decrease in Sb/Ag ratio in δ-matrix taking place with aging time at temperatures below δ-solvus, it is expected that electrical conductivity of two-phase δ+Sb_2Te_3 alloy should increase with aging time, disregarding effects, such as electron boundary scattering. Interestingly, these two effects have opposite consequences regarding Seebeck coefficient, so that, it is difficult to assess resulting Seebeck coefficient.

http://dx.doi.org/10.5772/66086

Experimentally, model ternary ($AgSbTe_2$) and quaternary (3 at.% La-$AgSbTe_2$) alloys were synthesized by vacuum melting followed by quenching and hot-pressing. The appropriate conditions enabling formation of $AgSbTe_2$-matrix that dissolves La-atoms with no La-rich precipitates were established. DSC tests enable observation of $Ag_2Te+Sb_2Te_3 \rightarrow \delta$-$AgSbTe_2$ phase transition at 360°C for La-free alloys only, indicating improvement of alloy's thermal stability due to La-additions. Temperature-dependent thermal conductivity of both alloys indicate reduction in thermal conductivity as a result of La-alloying from 0.92 to 0.71 W m^{-1} K^{-1} at 573 K, which corresponds with the trend predicted from first-principles. Measurements of temperature-dependent electrical conductivity and Seebeck coefficients indicate that La-doping reduces electrical conductivity and increases Seebeck coefficients, as predicted from first-principles. Eventually, it is shown that La-doping has positive effects on TE figure-of-merit *ZT*, which is improved, e.g., from 0.35 up to 0.50 at 260°C.

We demonstrate how first-principles calculations serve as trustworthy tool for predicting TE performance of materials, screening the best candidates for application in TE devices. It is noteworthy that such DFT routines prove to be very efficient by prediction of TE properties in a way saving expensive and time-consuming experiments. The resulting materials that seem to possess improved performance are, eventually, processed in laboratory. We show how simple physical considerations can be implemented in DFT calculations and lead to improvement of power conversion efficiency. La-doping improves the alloys' thermal stability and reduces their thermal conductivity, as well as enhances TE power factor in certain temperature range. As a result, the total TE figure-of-merit improves significantly. We, finally, emphasize the universal aspects of this approach that can be applied for other TE materials, as well.

Acknowledgements

The author wishes to acknowledge generous support from the Israel Science Foundation (ISF), Grant no. 698/13, as well as, from the German-Israeli Foundation for Research and Development (GIF), Grant no. I-2333-1150.10/2012. Partial support from the Nancy and Stephen Grand Technion Energy Program (GTEP), the Russell Berrie Nanotechnology Institute (RBNI), Technion, and the Adelis Foundation for renewable energy research are greatly acknowledged, as well.

Author details

Yaron Amouyal

Address all correspondence to: amouyal@technion.ac.il

Department of Materials Science and Engineering, Technion—Israel Institute of Technology, Haifa, Israel

References

[1] Martin RM.: Electronic Structure – Basic Theory and Practical Methods. Cambridge, UK: Cambridge University Press; 2004.

[2] Argaman N, Makov G.: Density functional theory: An introduction. Am. J. Phys. 2000;**68**:69–79. doi:10.1119/1.19375

[3] Mishin Y, Asta M, Li J.: Atomistic modeling of interfaces and their impact on microstructure and properties. Acta. Mater. 2010;**58**:1117–51. doi:10.1016/j.actamat.2009.10.049

[4] Parr RG, Yang W.: Density-Functional Theory of Atoms and Molecules. New York: Oxford University Press; 1989.

[5] Hsu KF, Loo S, Guo F, Chen W, Dyck JS, Uher C, Hogan T, Polychroniadis EK, Kanatzidis MG.: Cubic $AgPb_mSbTe_{2+m}$: bulk thermoelectric materials with high figure of merit. Science. 2004;**303**:818–821. doi:10.1126/science.1092963

[6] Kanatzidis MG.: Nanostructured thermoelectrics: The new paradigm? Chem. Mater. 2010;**22**:648–659. doi:10.1021/cm902195j

[7] Dadda J, Muller E, Klobes B, Pereira PB, Hermann R.: Electronic properties as a function of Ag/Sb ratio in $Ag_{1-y}Pb_{18}Sb_{1+z}Te_{20}$ compounds. J. Electron. Mater. 2012;**41**:2065–72. doi:10.1007/s11664-012-2111-9

[8] Dadda J, Muller E, Perlt S, Hoche T, Pereira PB, Hermann RP.: Microstructures and nanostructures in long-term annealed $AgPb_{18}SbTe_{20}$ (LAST-18) compounds and their influence on the thermoelectric properties. J. Mater. Res. 2011;**26**:1800–1812. doi:10.1557/jmr.2011.142

[9] Perlt S, Hoche T, Dadda J, Muller E, Pereira PB, Hermann R, Sarahan M, Pippel E, Brydson R.: Microstructure analyses and thermoelectric properties of $Ag_{1-x}Pb_{18}Sb_{1+y}Te_{20}$. J. Solid State Chem. 2012;**193**:58–63. doi:10.1016/j.jssc.2012.03.064

[10] Cook BA, Kramer MJ, Harringa JL, Han MK, Chung DY, Kanatzidis MG.: Analysis of nanostructuring in high figure-of-merit $Ag_{1-x}Pb_mSbTe_{2+m}$ thermoelectric materials. Adv. Funct. Mater. 2009;**19**:1254–1259. doi:10.1002/adfm.200801284

[11] Sootsman JR, Chung DY, Kanatzidis MG.: New and old concepts in thermoelectric materials. Angew. Chem-Int. Edit. 2009;**48**:8616–8639. doi:10.1002/anie.200900598

[12] Steimer C, Welnic W, Kalb J, Wuttig M.: Towards an atomistic understanding of phase change materials. J. Optoelectron. Adv. Mater. 2006;**8**:2044–2050.

[13] Wang K, Steimer C, Detemple R, Wamwangi D, Wuttig M.: Assessment of Se based phase change alloy as a candidate for non-volatile electronic memory applications. Appl. Phys. A. 2005;**81**:1601–1605. doi:10.1007/s00339-005-3358-2

[14] Siegert KS, Lange FRL, Sittner ER, Volker H, Schlockermann C, Siegrist T, Wuttig M.: Impact of vacancy ordering on thermal transport in crystalline phase-change materials. Rep. Prog. Phys. 2015;**78**:013001. doi:10.1088/0034-4885/78/1/013001

[15] Wuttig M, Yamada N.: Phase-change materials for rewriteable data storage. Nat. Mater. 2007;**6**:1004. doi:10.1038/nmat2077

[16] Ma J, Delaire O, May AF, Carlton CE, McGuire MA, VanBebber LH, Abernathy DL, Ehlers G, Hong T, Huq A, Tian W, Keppens VM, Shao Horn Y, Sales BC.: Glass-like phonon scattering from a spontaneous nanostructure in $AgSbTe_2$. Nat. Nano. 2013;**8**:445–451. doi:10.1038/nnano.2013.95

[17] Specht ED, Ma J, Delaire O, Budai JD, May AF, Karapetrova EA.: Nanoscale structure in $AgSbTe_2$ determined by diffuse elastic neutron scattering. J. Electron. Mater. 2015;**44**:1536–9. doi:10.1007/s11664-014-3447-0

[18] Shinya H, Masago A, Fukushima T, Katayama-Yoshida H.: Inherent instability by antibonding coupling in $AgSbTe_2$. Jpn. J. Appl. Phys. 2016;**55**:6. doi:10.7567/jjap.55.041801

[19] Jovovic V, Heremans JP.: Doping effects on the thermoelectric properties of $AgSbTe_2$. J. Electron. Mater. 2009;**38**:1504–1509. doi:10.1007/s11664-009-0669-7

[20] Morelli DT, Jovovic V, Heremans JP.: Intrinsically minimal thermal conductivity in cubic I-V-VI_2 semiconductors. Phys. Rev. Lett. 2008;**101**:035901. doi:10.1103/PhysRevLett.101.035901

[21] Nielsen MD, Ozolins V, Heremans JP.: Lone pair electrons minimize lattice thermal conductivity. Energy Environ. Sci. 2013;**6**:570–578. doi:10.1039/C2EE23391F

[22] Ye L-H, Hoang K, Freeman AJ, Mahanti SD, He J, Tritt TM, Kanatzidis MG.: First-principles study of the electronic, optical, and lattice vibrational properties of $AgSbTe_2$. Phys. Rev. B. 2008;**77**:245203. doi:10.1103/PhysRevB.77.245203

[23] Lencer D, Salinga M, Grabowski B, Hickel T, Neugebauer J, Wuttig M.: A map for phase-change materials. Nat. Mater. 2008;**7**:972–977. http://www.nature.com/nmat/journal/v7/n12/suppinfo/nmat2330_S1.html

[24] Shportko K, Kremers S, Woda M, Lencer D, Robertson J, Wuttig M.: Resonant bonding in crystalline phase-change materials. Nat. Mater. 2008;**7**:653–658. doi:10.1038/nmat2226

[25] Du B, Li H, Xu J, Tang X, Uher C.: Enhanced figure-of-merit in Se-doped p-type $AgSbTe_2$ thermoelectric compound. Chem. Mater. 2010;**22**:5521–5527. doi:10.1021/cm101503y

[26] Ma H, Su T, Zhu P, Guo J, Jia X.: Preparation and transport properties of $AgSbTe_2$ by high-pressure and high-temperature. J. Alloys Compd. 2008;**454**:415–418. doi:10.1016/j.jallcom.2006.12.126

[27] Min BK, Kim BS, Kim IH, Lee JK, Kim MH, Oh MW, Park SD, Lee HW.: Electron transport properties of La-doped $AgSbTe_2$ thermoelectric compounds. Electron. Mater. Lett. 2011;**7**:255–260. doi:10.1007/s13391-011-0914-0

[28] Sharma PA, Sugar JD, Medlin DL.: Influence of nanostructuring and heterogeneous nucleation on the thermoelectric figure of merit in $AgSbTe_2$. J. Appl. Phys. 2010;**107**:113716. doi:10.1063/1.3446094

[29] Sugar JD, Medlin DL.: Precipitation of Ag_2Te in the thermoelectric material $AgSbTe_2$. J. Alloys Compd. 2009;**478**:75–82. doi:10.1016/j.jallcom.2008.11.054

[30] Pereira PB. Structure and Lattice Dynamics of Thermoelectric Complex Chalcogenides. Julich Forschungszentrum: Universite de Liege; 2012.

[31] Barabash SV, Ozolins V, Wolverton C.: First-principles theory of competing order types, phase separation, and phonon spectra in thermoelectric $AgPb_mSbTe_{m+2}$ alloys. Phys. Rev. Lett. 2008;**101**:155704. doi:10.1103/PhysRevLett.101.155704

[32] Hoang K, Mahanti SD, Salvador JR, Kanatzidis MG.: Atomic ordering and gap formation in Ag-Sb-based ternary chalcogenides. Phys. Rev. Lett. 2007;**99**:156403.doi:10.1103/PhysRevLett.99.156403

[33] Rezaei N, Hashemifar SJ, Akbarzadeh H.: Thermoelectric properties of $AgSbTe_2$ from first-principles calculations. J. Appl. Phys. 2014;**116**:103705. doi:10.1063/1.4895062

[34] Singh DJ, Terasaki I.: Thermoelectrics - nanostructuring and more. Nat. Mater. 2008;**7**:616–617. doi:10.1038/nmat2243

[35] Toberer ES, Zevalkink A, Snyder GJ.: Phonon engineering through crystal chemistry. J. Mater. Chem. 2011;**21**:15843–15852. doi:10.1039/c1jm11754h

[36] He JQ, Girard SN, Kanatzidis MG, Dravid VP.: Microstructure-lattice thermal conductivity correlation in nanostructured $PbTe_{0.7}S_{0.3}$ thermoelectric materials. Adv. Funct. Mater. 2010;**20**:764–772. doi:10.1002/adfm.200901905

[37] He JQ, Sootsman JR, Girard SN, Zheng JC, Wen JG, Zhu YM, Kanatzidis MG, Dravid VP.: On the origin of increased phonon scattering in nanostructured PbTe based thermoelectric materials. J. Am. Chem. Soc. 2010;**132**:8669–8675. doi:10.1021/ja1010948

[38] Kim W, Singer SL, Majumdar A, Zide JMO, Klenov D, Gossard AC, Stemmer S.: Reducing thermal conductivity of crystalline solids at high temperature using embedded nanostructures. Nano Lett. 2008;**8**:2097–2099. doi:10.1021/nl080189t

[39] Du B, Li H, Tang X.: Effect of Ce substitution for Sb on the thermoelectric properties of $AgSbTe_2$ compound. J. Electron. Mater. 2014;**43**:2384–2389. doi:10.1007/s11664-014-3076-7

[40] Du BL, Li H, Tang XF.: Enhanced thermoelectric performance in Na/Se doped p-type $AgSbTe_2$ compound. J. Inorg. Mater. 2011;**26**:680–684. doi:10.3724/sp.j.1077.2011.00680

[41] Du BL, Li H, Tang XF.: Enhanced thermoelectric performance in Na-doped p-type non-stoichiometric $AgSbTe_2$ compound. J. Alloys Compd. 2011;**509**:2039–2043. doi:10.1016/j.jallcom.2010.10.131

[42] Mohanraman R, Sankar R, Boopathi KM, Chou FC, Chu CW, Lee CH, Chen Y-Y.: Influence of In doping on the thermoelectric properties of an $AgSbTe_2$ compound with enhanced figure of merit. J. Mater. Chem A. 2014;**2**:2839–2844. doi: 10.1039/c3ta14547f

[43] Mohanraman R, Sankar R, Chou FC, Lee CH, Chen Y-Y.: Enhanced thermoelectric performance in Bi-doped p-type $AgSbTe_2$ compounds. J. Appl. Phys. 2013;**114**. doi:10.1063/1.4828478

[44] Wu H-j, Chen S-w, Ikeda T, Snyder GJ.: Reduced thermal conductivity in Pb-alloyed $AgSbTe_2$ thermoelectric materials. Acta Mater. 2012;**60**:6144–6151. doi:10.1016/j.actamat.2012.07.057

[45] Zhang H, Luo J, Zhu HT, Liu QL, Liang JK, Li JB, Liu GY.: Synthesis and thermoelectric properties of Mn-doped $AgSbTe_2$ compounds. Chin. Phys. B. 2012;**21**:6. doi:10.1088/1674-1056/21/10/106101

[46] Zhang H, Luo J, Zhu HT, Liu QL, Liang JK, Rao GH.: Phase stability, crystal structure and thermoelectric properties of Cu doped $AgSbTe_2$. Acta Phys. Sin. 2012;**61**:7.

[47] Zhang SN, Jiang GY, Zhu TJ, Zhao XB, Yang SH.: Doping effect on thermoelectric properties of nonstoichiometric $AgSbTe_2$ compounds. Int. J. Miner. Metall. Mater. 2011;**18**:352–356. doi:10.1007/s12613-011-0446-5

[48] Mohanraman R, Sankar R, Chou F-C, Lee C-H, Iizuka Y, Muthuselvam IP, Chen Y-Y: Influence of nanoscale Ag_2Te precipitates on the thermoelectric properties of the Sn doped P-type $AgSbTe_2$ compound. APL Mater. 2014;**2**:096114. doi:10.1063/1.4896435

[49] Du B, Xu J, Zhang W, Tang X.: Impact of in situ generated Ag_2Te nanoparticles on the microstructure and thermoelectric properties of $AgSbTe_2$ compounds. J. Electron. Mater. 2011;**40**:1249–53. doi:10.1007/s11664-011-1620-2

[50] Zhang SN, Zhu TJ, Yang SH, Yu C, Zhao XB.: Improved thermoelectric properties of $AgSbTe_2$ based compounds with nanoscale Ag_2Te in situ precipitates. J. Alloys Compd. 2010;**499**:215–220. doi:10.1016/j.jallcom.2010.03.170

[51] Du B, Yan Y, Tang X.: Variable-temperature in situ X-ray diffraction study of the thermodynamic evolution of $AgSbTe_2$ thermoelectric compound. J. Electron. Mater. 2015;**44**:2118–2123. doi:10.1007/s11664-015-3682-z

[52] Li HY, Jing HY, Han YD, Lu GQ, Xu LY, Liu T.: Interfacial evolution behavior of $AgSbTe_{2.01}$/nanosilver/Cu thermoelectric joints. Mater. Des. 2016;**89**:604–610. doi:10.1016/j.matdes.2015.09.163

[53] Wyzga PM, Wojciechowski KT.: Analysis of the influence of thermal treatment on the stability of $Ag_{1-x}Sb_{1+x}Te_{2+x}$ and Se-doped $AgSbTe_2$. J. Electron. Mater. 2016;**45**:1548–1554. doi:10.1007/s11664-015-4102-0

[54] Pei Y, Lensch-Falk J, Toberer ES, Medlin DL, Snyder GJ.: High thermoelectric performance in PbTe due to large nanoscale Ag_2Te precipitates and La doping. Adv. Funct. Mater. 2011;**21**:241–249. doi:10.1002/adfm.201000878

[55] Takagiwa Y, Pei Y, Pomrehn G, Snyder GJ.: Dopants effect on the band structure of PbTe thermoelectric material. Appl. Phys. Lett. 2012;**101**:092102–3. doi:10.1063/1.4748363

[56] Min B-K, Kim B-S, Oh M-W, Ryu B-K, Lee J-E, Joo S-J, Park S-D, Lee H-W, Lee H-s.: Effect of La-doping on $AgSbTe_2$ thermoelectric compounds. J. Korean Phys. Soc. 2016;**68**:164–169. doi:10.3938/jkps.68.164

[57] Amouyal Y.: On the role of lanthanum substitution defects in reducing lattice thermal conductivity of the $AgSbTe_2$ (P4/mmm) thermoelectric compound for energy conversion applications. Comput. Mater. Sci. 2013;**78**:98–103.doi:10.1016/j.commatsci.2013.05.027

[58] Amouyal Y.: Reducing lattice thermal conductivity of the thermoelectric compound $AgSbTe_2$ (P4/mmm) by lanthanum substitution: computational and experimental approaches. J. Electron. Mater. 2014;**43**:3772–3779. doi:10.1007/s11664-014-3145-y

[59] Quarez E, Hsu KF, Pcionek R, Frangis N, Polychroniadis EK, Kanatzidis MG.: Nanostructuring, compositional fluctuations, and atomic ordering in the thermoelectric materials $AgPb_mSbTe_{2+m}$. The myth of solid solutions. J. Am. Chem. Soc. 2005;**127**:9177–9190. doi:10.1021/ja051653o

[60] Kresse G, Furthmuller J.: Efficiency of ab-initio total energy calculations for metals and semiconductors using a plane-wave basis set. Comput. Mater. Sci. 1996;**6**:15–50. doi:10.1016/0927-0256(96)00008-0

[61] Kresse G, Furthmueller J.: Efficient iterative schemes for Ab Initio total-energy calculations using a plane-wave basis set. Phys. Rev. B: Condens. Matter Mater. Phys. 1996;**54**:11169–11186. doi:10.1103/PhysRevB.54.11169

[62] Kresse G, Hafner J.: Ab initio molecular-dynamics simulation of the liquid-metal-amorphous-semiconductor transition in Germanium. Phys. Rev. B: Condens. Matter Mater. Phys. 1994;**49**:14251–14269. doi:10.1103/PhysRevB.49.14251

[63] MedeA®: Materials Design, Inc. 2010;v. **2.74**. Angel Fire, NM, USA.

[64] Perdew JP, Ruzsinszky A, Csonka GI, Vydrov OA, Scuseria GE, Constantin LA, Zhou X, Burke K.: Restoring the density-gradient expansion for exchange in solids and surfaces. Phys. Rev. Lett. 2008;**100**:136406. doi:10.1103/PhysRevLett.100.136406

[65] Kresse G, Joubert D.: From ultrasoft pseudopotentials to the projector augmented-wave method. Phys. Rev. B. 1999;**59**:1758. doi:10.1103/PhysRevB.59.1758

[66] Blöchl PE, Jepsen O, Andersen OK.: Improved tetrahedron method for Brillouin-zone integrations. Phys. Rev. B. 1994;**49**:16223–16233. doi:10.1103/PhysRevB.49.16223

[67] Madsen GKH, Singh DJ.: BoltzTraP. A code for calculating band-structure dependent quantities. Comput. Phys. Commun. 2006;**175**:67–71. doi:10.1016/j.cpc.2006.03.007

[68] Scheidemantel TJ, Ambrosch-Draxl C, Thonhauser T, Badding JV, Sofo JO.: Transport coefficients from first-principles calculations. Phys. Rev. B. 2003;**68**:125210. doi:10.1103/PhysRevB.68.125210

[69] Ashcroft NW, Mermin ND. Solid State Physics: Holt, Rinehart and Winston; 1976.

[70] Joseph E, Amouyal Y.: Towards a predictive route for selection of doping elements for the thermoelectric compound PbTe from first-principles. J. Appl. Phys. 2015;**117**:175102. doi:10.1063/1.4919425

[71] Joseph E, Amouyal Y.: Enhancing thermoelectric performance of PbTe-based compounds by substituting elements: a first principles study. J. Electron. Mater. 2015;**44**:1460–1468. doi:10.1007/s11664-014-3416-7

[72] Poudeu PFP, Kanatzidis MG.: Design in solid state chemistry based on phase homologies. Sb_4Te_3 and Sb_8Te_9 as new members of the series $(Sb_2Te_3)_m{\cdot}(Sb_2)_n$. Chem. Commun. 2005:2672–2674. doi:10.1039/B500695C

[73] Kifune K, Fujita T, Kubota Y, Yamada N, Matsunaga T.: Crystallization of the chalcogenide compound Sb_8Te_3. Acta Crystallogr. Sect. B. 2011;**67**:381–385. doi:10.1107/S0108768111033738

[74] Amram D, Amouyal Y, Rabkin E.: Encapsulation by segregation – a multifaceted approach to gold segregation in iron particles on sapphire. Acta Mater. 2016;**102**:342–351. doi:10.1016/j.actamat.2015.08.081

[75] Ahmad S, Mahanti SD, Hoang K, Kanatzidis MG.: Ab initio studies of the electronic structure of defects in PbTe. Phys. Rev. B. 2006;**74**:155205. doi:10.1103/PhysRevB.74.155205

[76] Graff A, Amouyal Y.: Effects of lattice defects and niobium doping on thermoelectric properties of calcium manganate compounds for energy harvesting applications. J. Electron. Mater. 2016;**45**:1508–1516. doi:10.1007/s11664-015-4089-6

[77] de Boor J, Stiewe C, Ziolkowski P, Dasgupta T, Karpinski G, Lenz E, Edler F, Mueller E.: High-temperature measurement of seebeck coefficient and electrical conductivity. J. Electron. Mater. 2013;**42**:1711–1718. doi:10.1007/s11664-012-2404-z

[78] Edler F, Lenz E.: Metrology for energy harvesting. AIP Conference Proceedings. 2012;**1449**:369–372. doi:10.1063/1.4731573

[79] Cowan RD.: Pulse method of measuring thermal diffusivity at high temperatures. J. Appl. Phys. 1963;**34**:926–927. doi:10.1063/1.1729564

[80] Rowe DM.: Thermoelectrics Handbook: Macroto Nano. Boca Ravton: Taylor & Francis Group; 2006.

[81] Klemens PG.: The scattering of low-frequency lattice waves by static imperfections. Proc. Phys. Soc. Section A. 1955;**68**:1113.

[82] Klemens PG.: Thermal resistance due to point defects at high temperatures. Phys. Rev. 1960;**119**:507–509. doi:10.1103/PhysRev.119.507

[83] Abeles B.: Lattice thermal conductivity of disordered semiconductor alloys at high temperatures. Phys. Rev. 1963;**131**:1906–1911. doi:10.1103/PhysRev.131.1906

[84] Abeles B, Beers DS, Cody GD, Dismukes JP.: Thermal conductivity of Ge-Si alloys at high temperatures. Phys. Rev. 1962;**125**:44–46. doi:10.1103/PhysRev.125.44

[85] Hurd AJ, Kelly RL, Eggert RG, Lee M-H.: Energy-critical elements for sustainable development. MRS Bull. 2012;**37**:405–410. doi:10.1557/mrs.2012.54

[86] Callaway J.: Model for lattice thermal conductivity at low temperatures. Phys. Rev. 1959;**113**:1046. doi:10.1103/PhysRev.113.1046

[87] Callaway J, von Baeyer HC.: Effect of point imperfections on lattice thermal conductivity. Phys. Rev. 1960;**120**:1149. doi:10.1103/PhysRev.120.1149

[88] He J, Zhao L-D, Zheng J-C, Doak J, Wu H, Wang H-Q, Lee Y, Wolverton C, Kanatzidis M, Dravid V.: Role of sodium doping in lead chalcogenide thermoelectrics. J. Am. Chem. Soc. 2013;**135**:4624–4627. doi:10.1021/ja312562d

[89] He JQ, Girard SN, Zheng JC, Zhao LD, Kanatzidis MG, Dravid VP.: Strong phonon scattering by layer structured $PbSnS_2$ in PbTe based thermoelectric materials. Adv. Mater. 2012;**24**:4440–4444. doi:10.1002/adma.201201565

[90] Kim W, Zide J, Gossard A, Klenov D, Stemmer S, Shakouri A, Majumdar A.: Thermal conductivity reduction and thermoelectric figure of merit increase by embedding nanoparticles in crystalline semiconductors. Phys. Rev. Lett. 2006;**96**:045901. doi:10.1103/PhysRevLett.96.045901

[91] Wu LJ, Zheng JC, Zhou J, Li Q, Yang JH, Zhu YM.: Nanostructures and defects in thermoelectric $AgPb_{18}SbTe_{20}$ single crystal. J. Appl. Phys. 2009;**105**: 094317. doi:10.1063/1.3124364

[92] Lo S-H, He J, Biswas K, Kanatzidis MG, Dravid VP.: Phonon scattering and thermal conductivity in p-type nanostructured PbTe-BaTe bulk thermoelectric materials. Adv. Funct. Mater. 2012;**22**:5175–5184. doi:10.1002/adfm.201201221

[93] Graff A, Amouyal Y.: Reduced thermal conductivity in niobium-doped calcium-manganate compounds for thermoelectric applications. Appl. Phys. Lett. 2014;**105**:181906. doi:10.1063/1.4901269

[94] Goldsmid HJ.: Introduction to Thermoelectricity. Heidelberg Dordrecht London New York: Springer-Verlag; 2009.

[95] Tritt TM. Thermal Conductivity: Theory, Properties, and Applications. Clemson University, Clemson: Kluwer Academic/Plenum Publishers; 2004.

[96] Tritt TM.: Thermoelectric phenomena, materials, and applications. Annu. Rev. Mater. Res. 2011;**41**:433–448. doi:10.1146/annurev-matsci-062910-100453

[97] Morelli DT, Heremans JP, Slack GA.: Estimation of the isotope effect on the lattice thermal conductivity of group IV and group III-V semiconductors. Phys. Rev. B. 2002;**66**:195304. doi:10.1103/PhysRevB.66.195304

[98] Jovovic V, Heremans JP.: Measurements of the energy band gap and valence band structure of $AgSbTe_2$. Phys. Rev. B. 2008;**77**:245204. doi:10.1103/PhysRevB.77.245204

[99] Du BL, Li H, Xu JJ, Tang XF, Uher C.: Enhanced thermoelectric performance and novel nanopores in $AgSbTe_2$ prepared by melt spinning. J. Solid State Chem. 2011;**184**:109–114. doi:10.1016/j.jssc.2010.10.036

[100] Medlin DL, Sugar JD.: Interfacial defect structure at Sb_2Te_3 precipitates in the thermoelectric compound $AgSbTe_2$. Scripta Materialia. 2010;**62**:379–382. doi:10.1016/j.scriptamat.2009.11.028

[101] Zhang SN, Zhu TJ, Yang SH, Yu C, Zhao XB.: Phase compositions, nanoscale microstructures and thermoelectric properties in $Ag_{2-y}Sb_yTe_{1+y}$ alloys with precipitated Sb_2Te_3 plates. Acta Mater. 2010;**58**:4160–4169. doi:10.1016/j.actamat.2010.04.007

[102] Ayral-Marin RM, Brun G, Maurin M, Tedenac JC.: Contribution to the study of $AgSbTe_2$. Euro. J. Solid State Chem. 1990;**27**:747–757.

[103] Wu H-J, Chen S-W.: Phase equilibria of Ag–Sb–Te thermoelectric materials. Acta Mater. 2011;**59**:6463–6472. doi:10.1016/j.actamat.2011.07.010

[104] Sugar JD, Medlin DL.: Solid-state precipitation of stable and metastable layered compounds in thermoelectric $AgSbTe_2$. J. Mater. Sci. 2011;**46**:1668–1679. doi:10.1007/s10853-010-4984-4

[105] Kifune K, Fujita T, Tachizawa T, Kubota Y, Yamada N, Matsunaga T.: Crystal structures of X-phase in the Sb–Te binary alloy system. Cryst. Res. Technol. 2013;**48**:1011–1021. doi:10.1002/crat.201300252

[106] Kifune K, Kubota Y, Matsunaga T, Yamada N.: Extremely long period-stacking structure in the Sb-Te binary system. Acta Crystallographica. Section B. 2005;**61**:492–497. doi:10.1107/S0108768105017714

[107] Shelimova LE, Karpinskii OG, Kretova MA, Kosyakov VI, Shestakov VA, Zemskov VS, Kuznetsov FA.: Homologous series of layered tetradymite-like compounds in the Sb-Te and GeTe-Sb_2Te_3 systems. Inorg. Mater. 2000;**36**:768–775. doi:10.1007/bf02758595

[108] Sutton AP, Balluffi RW. Interfaces in Crystalline Materials, Oxford: Clarendon Press; 1995.

[109] Porter DA, Easterling KE. Phase Transformations in Metals and Alloys. 2ndEd. London: Chapman & Hall; 1992.

[110] Stowe K.: Crystal structure and electronic band structure of $LaTe_2$. J. Solid State Chem. 2000;**149**:155–166. doi:10.1006/jssc.1999.8514

[111] Chen Y, He B, Zhu TJ, Zhao XB.: Thermoelectric properties of non-stoichiometric $AgSbTe_2$ based alloys with a small amount of GeTe addition. J. Phys. D: Appl. Phys. 2012;**45**:115302. doi:10.1088/0022-3727/45/11/115302

[112] Chen Y, Nielsen MD, Gao YB, Zhu TJ, Zhao XB, Heremans JP.: SnTe-$AgSbTe_2$ thermoelectric alloys. Adv. Energy Mater. 2012;**2**:58–62. doi:10.1002/aenm.201100460

[113] Su T, Jia X, Ma H, Yu F, Tian Y, Zuo G, Zheng Y, Jiang Y, Dong D, Deng L, Qin B, Zheng S.: Enhanced thermoelectric performance of $AgSbTe_2$ synthesized by high pressure and high temperature. J. Appl. Phys. 2009;**105**: 3106102. doi:10.1063/1.3106102